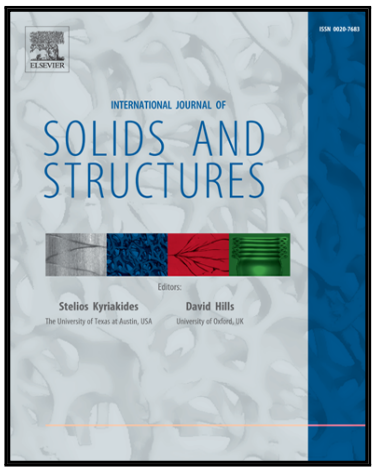

Full contact analysis of wire rope strand subjected to varying loads based on semi-analytical method

Yuanpei Chen , Fanming Meng , Xiansheng Gong

PII: S0020-7683(17)30153-1
DOI: 10.1016/j.ijsolstr.2017.04.004
Reference: SAS 9527

To appear in: *International Journal of Solids and Structures*

Received date: 7 September 2016
Revised date: 9 March 2017
Accepted date: 2 April 2017

Please cite this article as: Yuanpei Chen , Fanming Meng , Xiansheng Gong , Full contact analysis of wire rope strand subjected to varying loads based on semi-analytical method, *International Journal of Solids and Structures* (2017), doi: 10.1016/j.ijsolstr.2017.04.004

Highlights

- The behavior of wire strand under varying axial tension and torsion is analyzed.
- An interwire full contact model considering different contact statuses is built.
- The coupled contact status happens to the strands under some certain axial loads.
- The stiffness at a large lay angle increases obviously with increasing axial load.

Full contact analysis of wire rope strand subjected to varying loads based on semi-analytical method

Yuanpei Chen[a], Fanming Meng[a,*], Xiansheng Gong[b]

[a] *The State Key Laboratory of Mechanical Transmission, Chongqing University, Chongqing 400044, China*

[b] *College of Mechanical Engineering, Chongqing University, Chongqing 400044, China*

* Corresponding author: Fanming Meng. Tel: +86 023 65111482

E-mail address: fmmeng412@163.com (F.M. Meng)

Abstract

A wire rope is often subjected to a varying axial tensile force or torsional moment, resulting in its unstable performances. However, this problem has not been studied to date due to the lack of a scheme effectively determining the interwire contact status. For this, an interwire full contact model considering different contact statuses is established based on contact mechanic and thin rods theories. Then the model is solved with the semi-analytical method (SAM), into which the conjugate gradient method (CGM) and fast Fourier transform (FFT) are employed for analyzing the contact behavior. With the above contact dealing, the full contact performances are achieved for the core-wire contact, the wire-wire contact and the coupled contact statuses of the strand subjected to varying axial loads. And it is found that the interwire contact status of the strand may change with the varying loads, resulting in the unstable distributions of the interwire contact pressure and deformation. Meanwhile, the validity of the proposed full contact model is verified.

Keywords

Full contact; Wire rope strand; Stiffness; Axial loads; Semi-analytical method

1. Introduction

A wire rope is used in many applications, such as elevator, hoisting crane, suspension bridge and mine hoisting. Besides a remarkable tensile strength, the relative small bending and torsional stiffness make the rope easy to be wounded around a sheave or winding drum, which is beneficial to simplify the structures that the rope involved. Many wire ropes, like the ones for lifting, work under the circumstances of heavy loads. Any failure of the rope may lead to serious consequences, showing that the research on the rope is very significant.

To date, there have been many analytical studies on the mechanical performance of the wire rope, most of which were conducted based on the hypothesis of linear elastic. According to the reciprocity theorem of Betti (Samras et al., 1974), the stiffness matrix showing the relation between the axial strains and the external axial loads of the rope should be symmetric. Considering the extension of wires in a wire rope strand, Hruska (1952, 1953) studied the mechanical property of a wire strand, and a strictly symmetric stiffness matrix was obtained. However, the torsion and bending of the wires were not included in his works. The torsion performance of the wires in the strand was considered by Mcconnell and Zemke (1982), who pointed out that the properties of extension and torsion of the strand affect each other. Besides, the symmetry of the stiffness matrix by Mcconnell and Zemke was lost. By projecting the bending and torsion moments of the wires to the strand's axis, Machida and Durelli (1973) studied the influence of the wire's bending and torsion on the stiffness of the strand, and they also derived an asymmetric stiffness matrix. Based on Costello's (1983) work that considers the tension, torsion, bending and Poisson's ratio effect of the wires, Kumar and Cochran (1987) obtained a closed-form solution for the asymmetric stiffness matrix of the wire rope strand. According to Costello's model, the cross-sectional moments of the wire are proportional to the changes in the curvature and torsion. This dealing was improved by Ramsey (1988) using a differential geometric method, and the said moments were thought to depend on not only the above-mentioned changes but also the values of the curvature and torsion. Meanwhile, both the stiffness matrixes by Costello and

Ramsey are asymmetric. On the basis of the discrete thin rods theory, Sathikh et al. (1996) established a linear elastic model and achieved a closed-form symmetric stiffness matrix of a wire rope strand. However, the compressibility of the strand core was ignored. The study from Ghoreishi et al. (2007) shows that early models involving the axial strand performances have limitations in real applications due to the used assumptions (Jolicoeur and Cardou, 1991), such as the wire rope strand is assumed as a linear elastic system.

Besides the performance of the simple straight wire rope strand, the mechanical property of wire rope with multi-stand has also been studied so far. Costello (1997) dealt with the spiral strand as a one-order discrete thin rod. Elata et al. (2004) made a wire level analysis on the mechanical property of a multi-strand wire rope. However, a "fiber model" was adopted to model the second order helix wire in their study, without the consideration of the effects of the bending, torsion and Poisson's ratio of the wire. Using a hierarchical approach, Inagaki et al. (2007) established a model of a second order helix wire and analyzed the usage life of the wires. Nevertheless, the radial compression of the wire was ignored. Based on the beam hypotheses and thin rods theory, Usabiaga and Pagalday (2008) modeled the helical wires of first and second orders in a wire rope with a recursive method, without the consideration of the effect of Poisson's ratio of wires. Spak et al. (2013) conducted an overview on the research progress of wire rope with single and multiple strands, and pointed out that the damping property caused by the friction and viscoelastic shear effect should be incorporated in modeling wire ropes. Wang et al. (2015) derived the recursive expressions of the wires and strand in a wire rope, and the recursive method can be adopted to model a wire rope with any form of rope axis. The properties of extension, torsion and bending and the effect of the Poisson's ratio of the wire have been studied in the above-mentioned researches. In real situation, external loads on the wire rope may result in the interwire contact. The deformation caused by the interwire contact changes the wire's relative location and interwire clearance, and further influences the mechanical performance of the wire rope. However, the interwire contact has not been incorporated in the said studies.

On the other hand, some studies considering the contact problem of wire rope have been conducted.

Kumar and Botsis (2001) calculated the maximum stress of a multi-layer wire rope strand subjected to axial tensile and twist moment by use of Hertz theory. And their results show that the elastic modulus has an obvious influence on the contact stress of the wire. The initial contact between adjacent wires was considered by Prakash et al. (1992), who calculated the bending stiffness of a wire rope strand. Usabiaga et al. (2008) experimentally measured the normal contact force between a winding wire rope and sheave. By using the finite element method (FEM), Jiang et al. (2008) conducted a simulation analysis on a wire rope strand under a constrained torsion condition, and solved the statically indeterminate contact problem. The influence of the friction on the coupled contact performance of a wire rope strand was studied by Gnanavel et al. (2010), with the adoptions of the equilibrium equation and the Hertz elastic contact theory. Argatov (2011) modeled and analyzed the interwire contact property of a wire rope strand subjected to axial and torsional loads, using an asymptotic method. Based on the concept "p-extension" and a high-order nonlinear spring element in finite element theory, the nonlinear contact in a wire rope strand under small deformation condition was modeled by Paczelt and Beleznai (2011). With the adoption of Frenet–Serret frame and principal torsion-flexure axes, Xiang et al. (2015) deduced the influences of axial extension and torsion loads on the special positions of steel wires in first and second order helix, and studied the wire deformation and stress caused by the axial loads. Their work shows that the contact deformation strongly affects the local stress in wires. Besides the above-mentioned works, the interwire contact of the wire rope has also been simulated by other researchers with FEM (Chen et al., 2015; Erdonmez and Imrak, 2011; Fontanari et al., 2015; Jiang, 2012; Jiang and Henshall, 1999; Jiang et al., 1999; Stanova et al., 2015; Yu et al., 2014). The nonlinear factors, such as the interwire contact and the elasto-plasticity of wire, have also been considered. To achieve the numerical precision, nevertheless, dense meshes need to be generated, leading to a heavy computation burden. And the solution convergence for the nonlinear interwire contact problem may be hard to realize.

In addition, the constant contact status between wires was used in the past researches. In real operation

conditions, however, the load acting on the wire ropes is usually not constant, and the change in the load may cause a varying interwire contact status of the wire rope. The changeable phenomenon was also mentioned by Gnanavel et al. (2010), who however ignored the interwire contact deformation and did not make a deep study on the changeable interwire contact status at varying loads. In view of that the varying interwire contact status has not been analyzed in the past researches, therefore, a deep analysis of it is of significance for a better deign and maintenance of the wire rope under varying loads.

To study the interwire contact at varying loads, some difficulties need to be overcome. First, one needs the precise solution method analyzing the interwire contact performance parameters, such as the contact pressure and contact deformation. This has been accomplished in the recent work of the present authors (Meng et al., 2016) with the adoption of the semi-analytical method (SAM). In the solution process with SAM, the influence coefficients of the interwire contact deformation due to the contact pressure are analytically obtained first, and then the contact pressure and contact deformation are calculated by the use of conjugate gradient method (CGM) (Polonsky and Keer, 1999) and fast Fourier transform (FFT) (Liu et al., 2000), respectively. In addition, the precise evaluation on the contact status between the wires is also needed. Although the contact problem of the wire rope was researched in the past years based on the assumption of the constant interwire contact status of the wire rope, a scheme analyzing different interwire contact behaviors (i.e., full contact) under varying loads has been desired to date. Aiming at this problem, an interwire full contact model considering different contact statuses is established in this paper. Based on this model, the change in the interwire contact status of the strand under varying loads can be precisely determined. Then the interwire contact behaviors at different contact statuses are studied based on the said semi-analytical method. Finally, some conclusions are obtained with the full contact analysis.

2. Full contact model

2.1. Basic parameters

The geometrical feature of a wire rope strand investigated in the present study is given in Fig. 1a, in

which the symbol h denotes the strand length in undeformed state. The α_2 and r_{h2} are the initial helix angle and initial helix radius of the outside wire centerline, respectively. The R_1 and R_2 are the initial radii of the central wire and the outside wire, respectively. As shown in Fig. 1a, the tensile strain ε_t of the strand subjected to an axial tensile force and torsional moment is defined as

$$\varepsilon_t = \left(\bar{h} - h\right)/h \tag{1}$$

where the $\bar{h}$ refers to the length of the deformed strand. The torsional strain τ_t of the strand due to the said axial loads is

$$\tau_t = \Delta\varphi/h \tag{2}$$

where the $\Delta\varphi$ represents the relative rotating angle between the two ends of the strand.

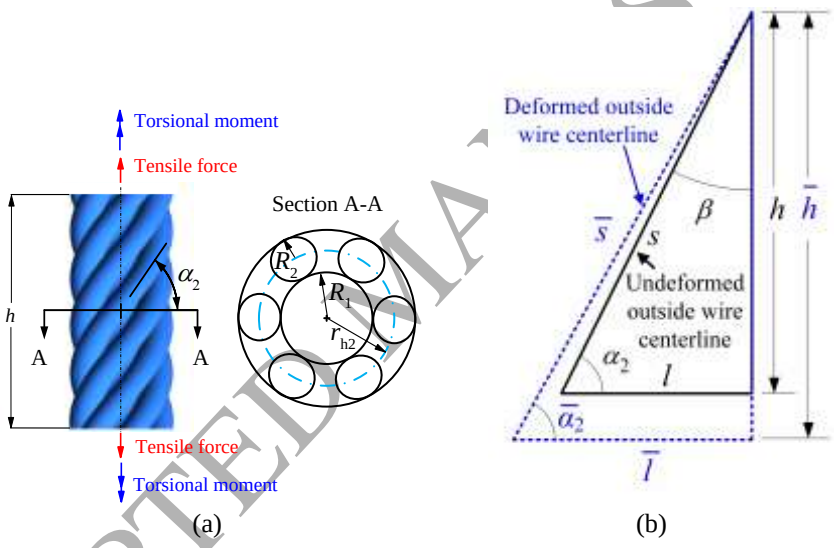

Fig. 1. Geometrical features. (a) Wire rope strand. (b) Outside wire centerline.

The schematic of the outside wire centerline of the strand is given in Fig. 1b, in which the symbol s is the length of the centerline, and l is the projection length of the centerline on the normal plane of the strand axis. The lay angle β is the complementary angle of the helix angle α_2 (i.e., β=90°-α_2). The barred symbols refer to the values considering the deformation of the strand, and it is the same for what follows. For the deformation characteristics and the geometrical relations of the strand, the axial tensile strain ξ_2 and the helix angle $\bar{\alpha}_2$ of the outside wire are respectively derived as (Meng et al., 2016)

$$\xi_2 = \sin\alpha_2 \sqrt{\left(\frac{\bar{r}_{h2}}{r_{h2}}\right)^2 \left(\cot\alpha_2 + r_{h2}\tau_t\right)^2 + \left(1+\varepsilon_t\right)^2} - 1 \tag{3}$$

$$\bar{\alpha}_2 = \arcsin\frac{\sin\alpha_2\left(1+\varepsilon_t\right)}{\left(1+\xi_2\right)} \tag{4}$$

where $\bar{r}_{h2}$ is the helix radius of the deformed outside wire centerline.

In real operation conditions, the interwire contact status probably change due to varying axial loads, which has not been considered in past researches (Argatov, 2011; Ghoreishi et al., 2007; Usabiaga and Pagalday, 2008). In view of the structural feature of the wire rope strand, the possible contact statuses between wires of the strand under a specific axial load are given in Fig. 2, in which the central wire and outside wire are denoted with symbols "CW" and "OW", respectively. According to the position where the interwire contact happens (see the contact line in Fig. 2), there exist three cases of the interwire contact status, which are the core-wire contact status (contact only happens between the central and outside wires, see Fig. 2a), the wire-wire contact status (contact only happens between the adjacent outside wires, see Fig. 2b) and the coupled contact status (both core-wire contact and wire-wire happen, see Fig. 2c). Different from the dealing that the interwire contact status was assumed as constant in past researches, the above three contact statuses are determined with a full contact model in the present study.

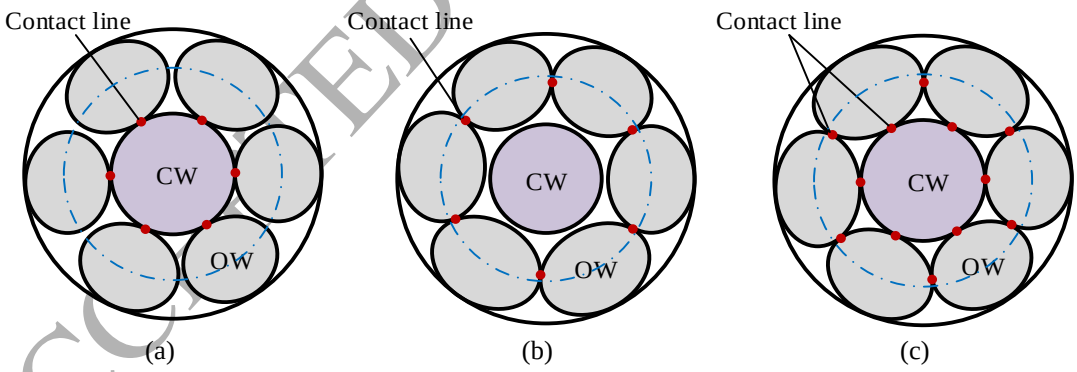

Fig. 2. Interwire contact statuses of wire rope strand. (a) Core-wire contact status. (b) Wire-wire contact status. (c) Coupled contact status.

To establish the full contact model, the geometrical parameters should be derived according to the interwire contact status of the strand. In the undeformed state, the initial helix radius r_{h2} of the outside wire centerline depends on the initial interwire contact status of the strand:

$$r_{h2} = r_{c\text{-}w},\ \text{if}\ r_{c\text{-}w} \geq r_{w\text{-}w} \tag{5a}$$

$$r_{h2} = r_{w\text{-}w},\ \text{if}\ r_{c\text{-}w} < r_{w\text{-}w} \tag{5b}$$

which means that Eq. (5a) is adopted if the initial interwire contact status is core-wire contact or coupled contact, and $r_{c\text{-}w}=R_1+R_2$. Meanwhile, if the initial wire-wire contact happens, the value of r_{h2} is evaluated with Eq. (5b), and $r_{w\text{-}w}=R_2\sqrt{1+\tan^2\left(\pi/2-\pi/m_2\right)/\sin^2\alpha_2}$. The symbol m_2 is the amount of the outside wire of the strand. It should be mentioned that the helix angle has an effect on the boundary shape of the outside wire in the cross-section of the strand, which has been reported by Karathanasopoulos and Angelikopoulos (2016) and Frikha et al. (2013). However, the said boundary shape can be assumed to be an ellipse for the wire strands with helix angles normally used, according to the researches by Costello (1997), Feyrer (2007) and Ghoreishi et al. (2007).

With the consideration of the Poisson's ratio and the flattening effect caused by the interwire contact deformation, the values of the axial strain ξ_2 and helix angle $\bar{\alpha}_2$ of the outside wire centerline in the deformed state also depend on the interwire contact status of the strand, which is different from the dealings in the past studies (Argatov, 2011; Usabiaga and Pagalday, 2008) based on the assumption of constant contact status.

In the case of core-wire contact, the final helix radius $\bar{r}_{h2}$ of the outside wire centerline is expressed as

$$\bar{r}_{h2}=\bar{R}_1+\bar{R}_2-\delta_1-\delta_2 \tag{6}$$

where the radii of the central and outside wires are $\bar{R}_1=R_1\left(1-\nu_1\xi_1\right)$ and $\bar{R}_2=R_2\left(1-\nu_2\xi_2\right)$, respectively. The ν is the Poisson's ratio of a wire. The axial strain of the central wire ξ_1 is equal to ε_t. δ is the contact deformation caused by the core-wire contact. And the subscripts 1 and 2 represent the central wire and the outside wire, respectively. According to Eqs. (3), (5) and (6), it yields

$$\xi_2=\frac{\sqrt{\left(\Phi\Gamma\Upsilon+1\right)^2+\left(1-\Upsilon\Gamma^2\right)\left(\Upsilon\Phi^2+\Psi-1\right)}-\left(\Phi\Gamma\Upsilon+1\right)}{\left(1-\Upsilon\Gamma^2\right)} \tag{7}$$

where the intermediate variables are defined as $\Phi=\left(R_1+R_2-R_1\nu_1\xi_1-\delta_1-\delta_2\right)/r_{h2}$, $\Gamma=R_2\nu_2/r_{h2}$, $\Upsilon=\left(\cot\alpha_2+r_{h2}\tau_t\right)^2\sin^2\alpha_2$ and $\Psi=\left(1+\varepsilon_t\right)^2\sin^2\alpha_2$. Then the helix angle $\bar{\alpha}_2$ of the outside wire centerline in the deformed state can be computed through Eq. (4).

In the case of wire-wire contact status, the deformation of the wire-wire contact in the normal plane of the

contact line is assumed to be δ_3. As shown in Fig. 3a, the wire-wire contact deformation δ_4 in the outside wire's cross-section is

$$\delta_4 = \delta_3 \cos\bar{\theta} \tag{8}$$

where the angle variable $\bar{\theta}$ is defined as $\bar{\theta} = \bar{\alpha}_{c2} - \bar{\alpha}_2$, and the helix angle of the wire-wire contact line $\bar{\alpha}_{c2}$ is calculated with

$$\bar{\alpha}_{c2} = \arctan\frac{\bar{p}_2}{2\pi\bar{r}_{c2}} \tag{9}$$

Here, the lay length of the deformed outside wire is $\bar{p}_2 = 2(1+\varepsilon_t)\pi r_{h2}\tan\alpha_2$. The symbol $\bar{r}_{c2}$ is the helix radius of the wire-wire contact line (see Fig. 3b) and expressed as (Costello, 1997)

$$\bar{r}_{c2} = \frac{\bar{R}_2\tan(\pi/2-\pi/m_2)}{\sin\bar{\alpha}_2\cos(\pi/2-\pi/m_2)\sqrt{\sin^2\bar{\alpha}_2+\tan^2(\pi/2-\pi/m_2)}} - \delta_5\cot(\pi/m_2) \tag{10}$$

where the deformation δ_5 in the strand's cross section due to the wire-wire contact is

$$\delta_5 = \frac{\delta_4}{\sin\bar{\alpha}_2} \tag{11}$$

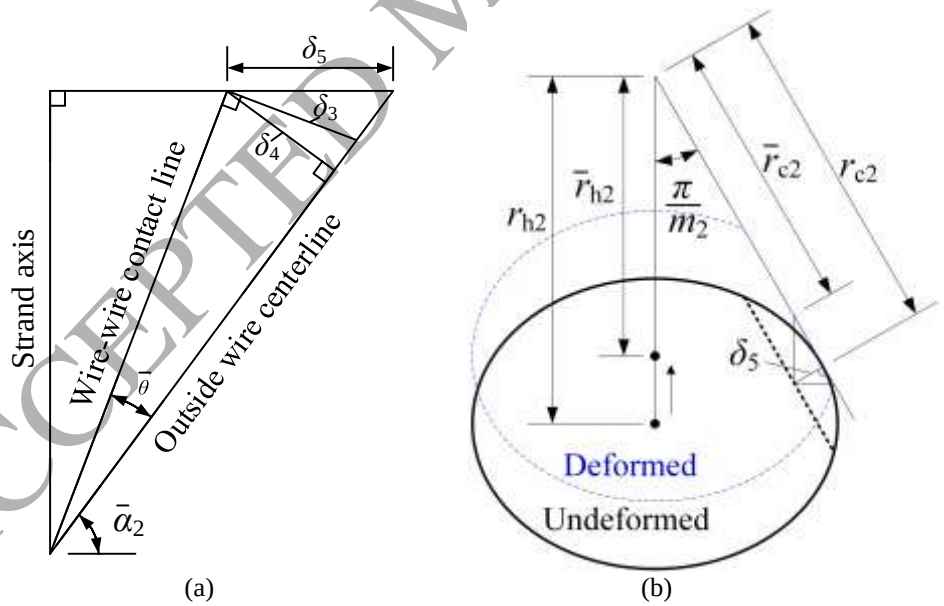

Fig. 3. Schematic of wire-wire contact. (a) Deformation relation. (b) Cross-section of strand.

Therefore, the helix radius of the deformed outside wire centerline in the case of wire-wire contact status is

$$\bar{r}_{h2} = \bar{R}_2\sqrt{1+\frac{\tan^2(\pi/2-\pi/m_2)}{\sin^2\bar{\alpha}_2}} - \frac{\delta_5}{\sin(\pi/m_2)} \tag{12}$$

where the first term is the value of the helix radius of deformed outside wire centerline only considering the Poisson's ratio, and the second term corresponds to the strand's radial rigid displacement due to the wire-wire contact deformation. According to Eqs. (3), (5) and (12), the axial strain of the outside wire in the wire-wire contact case can also be obtained with Eq. (7), in which two intermediate variables should be replaced with

$$\Phi = \frac{1}{r_{\mathrm{h}2}}\left[R_2\sqrt{1+\frac{\tan^2\left(\pi/2-\pi/m_2\right)}{\sin^2\bar{\alpha}_2}} - \frac{\delta_3\cos\bar{\theta}}{\sin\bar{\alpha}_2\sin\left(\pi/m_2\right)}\right] \tag{13a}$$

$$\Pi = \frac{1}{r_{\mathrm{h}2}}\left[R_2\nu_2\sqrt{1+\frac{\tan^2\left(\pi/2-\pi/m_2\right)}{\sin^2\bar{\alpha}_2}}\right] \tag{13b}$$

Eqs. (13a) and (13b) show that the values of the axial strain ξ_2 and the helix angle $\bar{\alpha}_2$ of the outside wire affect each other. The coupling solution of Eqs. (4) and (13) can be realized with an iterative method.

In the case of coupled contact status, both the mathematical derivations in the cases of core-wire contact and wire-wire contact are still valid. For simplifying the analysis, the derivations in the case of core-wire contact status are given for the coupled contact status.

As stated previously, the geometrical parameters of the strand under varying loads are calculated according to the interwire contact status, which can be judged with

$\bar{r}_{\text{c-w}} > \bar{r}_{\text{w-w}}$, core-wire contact status (14a)

$\bar{r}_{\text{c-w}} < \bar{r}_{\text{w-w}}$, wire-wire contact status (14b)

$\bar{r}_{\text{c-w}} = \bar{r}_{\text{w-w}}$, coupled contact status (14c)

where $\bar{r}_{\text{c-w}}$ and $\bar{r}_{\text{w-w}}$ are the helix radii when only the core-wire contact and wire-wire contact are considered, respectively. And the values of the said radii are expressed as

$$\bar{r}_{\text{c-w}} = R_1\left(1-\nu_1\xi_1\right)+R_2\left(1-\nu_2\xi_2\right)-\delta_1-\delta_2 \tag{15a}$$

$$\bar{r}_{\text{w-w}} = R_2\left(1-\nu_2\xi_2\right)\sqrt{1+\frac{\tan^2\left(\pi/2-\pi/m_2\right)}{\sin^2\bar{\alpha}_2}} - \frac{\delta_3\cos\bar{\theta}}{\sin\bar{\alpha}_2\sin\left(\pi/m_2\right)} \tag{15b}$$

Assume that the centerlines of the undeformed and deformed outside wires are both helical lines. The changes in the components of curvature (i.e., κ_2 and κ_2',) and the twist per unit length (τ_2) of the centerline

are respectively obtained with Eqs. (16a), (16b) and (16c):

$$\Delta\kappa_2 = \bar{\kappa}_2 - \kappa_2 = 0 \tag{16a}$$

$$\Delta\kappa_2' = \bar{\kappa}_2' - \kappa_2' = \frac{\cos^2\bar{\alpha}_2}{\bar{r}_{h2}} - \frac{\cos^2\alpha_2}{r_{h2}} \tag{16b}$$

$$\Delta\tau_2 = \bar{\tau}_2 - \tau_2 = \frac{\sin\bar{\alpha}_2\cos\bar{\alpha}_2}{\bar{r}_{h2}} - \frac{\sin\alpha_2\cos\alpha_2}{r_{h2}} \tag{16c}$$

2.2. Force equilibrium of outside wire

On the basis of the thin rods theory (Love, 1944), the mechanic performances for the strand subjected to varying loads is analyzed through an illustrated infinitesimal arc of the outside wire centerline shown in Fig. 4. In this figure, the global location is denoted with the e_x-e_y-e_z coordinate system. The symbols *x*, *y* and *z* represent the normal, binormal and tangential directions at any point on the centerline, respectively. The *x*- and *y*-directional components of the shearing force on a cross-section of the wire, and tensile force along the *z* direction are denoted with N_2, N_2' and T_2, respectively. The components of the cross-sectional bending moment about the *x*- and *y*-directions, and the twist moment about the *z* axis are represented with G_2, G_2' and H_2, respectively. The components of the line load per unit length of the outside wire centerline along the *x*-, *y*- and *z*-directions are denoted with symbols X_2, Y_2 and Z_2, respectively. The components of the moment per unit length of the outside wire centerline along the *x*-, *y*- and *z*-directions are denoted with K_2, K_2' and Θ_2, respectively. Based on the assumption used in the past literatures (Argatov, 2011; Costello, 1997), the tension, curvatures and torsion are thought to be constant along the centerline, and there is no bending moment acting on the outside wire. By ignoring the interwire friction, the force equilibrium of the outside wire is described as

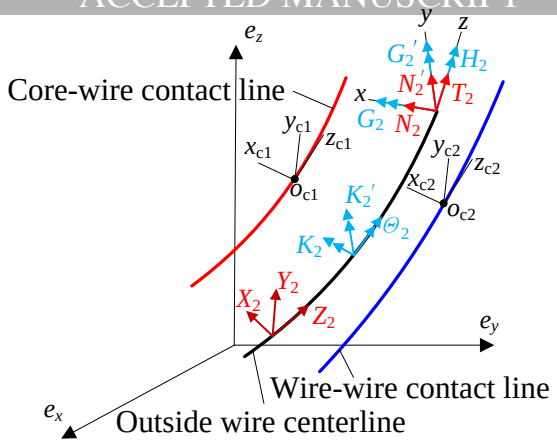

Fig. 4. Schematic of outside wire centerline and interwire contact lines.

$$-N_2'\bar{\tau}_2 + T_2\bar{\kappa}_2' + X_2 = 0 \tag{17a}$$

$$-G_2'\bar{\tau}_2 + H_2\bar{\kappa}_2' - N_2' = 0 \tag{17b}$$

According to the hypothesis of linear elastic theory, the tensile force of the outside wire in Eq. (17a) can be written as

$$T_2 = E_2\bar{A}_2\xi_2 \tag{18}$$

where E_2 and $\bar{A}_2$ are the Young's modulus and the cross-sectional area of the deformed outside wire, respectively. The values of the G_2, G_2' and H_2 can be obtained with the following relations (Ramsey, 1988):

$$G_2 = \frac{\pi E_2 \bar{R}_2^4}{4}\left(\Delta\kappa_2 + \kappa_2\xi_2\right) \tag{19a}$$

$$G_2' = \frac{\pi E_2 \bar{R}_2^4}{4}\left(\Delta\kappa_2' + \kappa_2'\xi_2\right) \tag{19b}$$

$$H_2 = \frac{\pi E_2 \bar{R}_2^4}{4(1+\nu)}\left(\Delta\tau_2 + \tau_2\xi_2\right) \tag{19c}$$

The axial force F and twist moment M acting on the strand are separately expressed as Eqs. (20a) and (20b):

$$F = \pi E_1 \bar{R}_1^2\xi_1 + m_2\left(T_2\sin\bar{\alpha}_2 + N_2'\cos\bar{\alpha}_2\right) \tag{20a}$$

$$M = \frac{\tau_t \pi E_1 \bar{R}_1^4}{4(1+\nu_1)} + m_2\left[\left(H_2 - N_2'\bar{r}_{h2}\right)\sin\bar{\alpha}_2 + \left(G_2' + T_2\bar{r}_{h2}\right)\cos\bar{\alpha}_2\right] \tag{20b}$$

where E_1 is the Young's modulus of the central wire. Besides, the values of all the geometrical variables in Eqs. (20a) and (20b) all consider the interwire contact, which is accordance with the real situation of the

loaded strand.

Based on the hypothesis of linear elastic and quasi-static, the axial deformation behavior of the strand can be expressed in the following form

$$\begin{Bmatrix} F \\ M \end{Bmatrix} = \begin{bmatrix} k_{\varepsilon\varepsilon} & k_{\varepsilon\theta} \\ k_{\theta\varepsilon} & k_{\theta\theta} \end{bmatrix} \begin{Bmatrix} \varepsilon_{\mathrm{t}} \\ \tau_{\mathrm{t}} \end{Bmatrix} \tag{21}$$

where the four stiffness matrix components $k_{\varepsilon\varepsilon}$, $k_{\theta\theta}$, $k_{\varepsilon\theta}$ and $k_{\theta\varepsilon}$ are axial tension, torsion and coupling terms, respectively. Once values of the F, M, and ε_{t} are known, the axial and coupling stiffnesses can be respectively calculated with $k_{\varepsilon\varepsilon}=F/\varepsilon_{\mathrm{t}}$ and $k_{\theta\varepsilon}=M/\varepsilon_{\mathrm{t}}$ under the condition of $\tau_{\mathrm{t}}=0$ rad/m. Similarly, the torsional stiffness $k_{\theta\theta}$ and the coupling stiffness $k_{\varepsilon\theta}$ can be respectively obtained with $k_{\theta\theta}=M/\tau_{\mathrm{t}}$ and $k_{\varepsilon\theta}=F/\tau_{\mathrm{t}}$ under the condition of $\varepsilon_{\mathrm{t}}=0$.

2.3. Interwire line contact load

As stated previously, the line load in Eq. (17a) acts on the outside wire centerline. The line action on the outside wire can be realized by the interwire contact. The interwire line contact load depends on the change in the interwire contact status in the full contact analysis of the strand subjected to varying loads, which is different from the situation of constant contact status used in the past researches (Argatov, 2011; Gnanavel et al., 2010).

In the case of the core-wire contact, the initial helix line contact zone between the central and outside wires becomes long and narrow due to the contact deformation. With a half width of b_1, the centerline of the deformed contact zone is defined as the core-wire contact line. The geometrical features of the core-wire contact line and the outside wire centerline indicate that the contact load per unit length of core-wire contact line (X_{c1}) can be obtain with (Costello, 1997)

$$X_{\mathrm{c1}} = -\frac{X_2}{k_1} \tag{22}$$

where the length ratio of the core-wire contact line to the outside wire centerline in the deformed state is defined as $k_1 = \sqrt{\bar{p}_2^2 + \left(2\pi\bar{r}_{\mathrm{c1}}\right)^2} \Big/ \sqrt{\bar{p}_2^2 + \left(2\pi\bar{r}_{\mathrm{h2}}\right)^2}$. Here, the $\bar{r}_{\mathrm{c1}}$ is the helix radius of the deformed core-wire

contact line, and $\bar{r}_{c1} = \bar{R}_1 - \delta_1$.

If the wire-wire contact occurs, on the other hand, the centerline of the deformed contact zone (with a half width of b_2) is used, defined as the wire-wire contact line. The load acting on the outside wire centerline is supplied by the contact interaction between the outside wires, and the contact load per unit length of wire-wire contact line (X_{c2}) is expressed as (Costello, 1997)

$$X_{c2} = -\frac{X_2}{2\cos\vartheta k_2} \tag{23}$$

where k_2 is the length ratio of the wire-wire contact line to the deformed outside wire centerline, defined as $k_2 = \sqrt{\bar{p}_2^2 + \left(2\pi\bar{r}_{c2}\right)^2} \Big/ \sqrt{\bar{p}_2^2 + \left(2\pi\bar{r}_{h2}\right)^2}$. The contact angle ϑ in Eq. (23) can be evaluated with the relation (Costello, 1997)

$$\cos\vartheta = \frac{1}{\cos^2\bar{\alpha}_2}\left\{\sqrt{1+\frac{\tan^2\left(\pi/2-\pi/m_2\right)}{\sin^2\bar{\alpha}_2}} - \sqrt{\tan^2\left(\frac{\pi}{2}-\frac{\pi}{m_2}\right)\left\{1+\frac{1}{\Xi_1}\right\}+\sin^4\bar{\alpha}_2}\right\} \tag{24}$$

where Ξ_1 is an intermediate variable, and $\Xi_1 = \tan^2\bar{\alpha}_2\cos^2\left(\pi/2-\pi/m_2\right)\left[\sin^2\bar{\alpha}_2 + \tan^2\left(\pi/2-\pi/m_2\right)\right]$.

Besides the above two contact statuses, the coupled contact status stated previously may occur at certain operation conditions. For this state, there exists a force balance between the line load per unit length of the outside wire centerline (X_2), the contact load per unit length of core-wire contact line (X_{c1}) and the contact load per unit length of wire-wire contact line (X_{c2}), which is written as

$$k_1 X_{c1} + 2\cos\vartheta k_2 X_{c2} = -X_2 \tag{25}$$

2.4. Interwire contact model

With respect to the interface where interwire contact happens, the normal Hertzian contact effect is considered. Meanwhile, the rotational stiffness effect at the interface of contact (Karathanasopoulos, 2015) is neglected based on the assumption that the wire surface is smooth. To establish the interwire contact model for the strand at varying loads, the expressions for the contact clearances of the core-wire contact and wire-wire contact are derived in this section. Then the load equilibrium between the line contact load and contact pressure, along with the relation between the contact pressure and the contact clearance, are given.

If the contact between the central and outside wires happens, infinitesimal segments of the central and outside wires with the length of d_{s0} along the contact line are taken for following derivations. As shown in Fig. 4, let o_{c1} denote an arbitrary point on the core-wire contact line, and respectively define lines $o_{c1}x_{c1}$, $o_{c1}y_{c1}$ and $o_{c1}z_{c1}$ as the normal, binomial and tangential directions of the core-wire contact line, respectively. Consequently, the core-wire contact clearance h_{c1} at a point (y_{c1}, z_{c1}) on the y_{c1} axis is obtained as

$$h_{c1}\left(y_{c1},z_{c1}\right)=h_{i1}\left(y_{c1},z_{c1}\right)+u_1\left(y_{c1},z_{c1}\right)-u_1\left(0,z_{c1}\right) \tag{26}$$

where h_{i1} is the initial clearance between the central and outside wires. The symbol u_1 denotes the total elastic deformation of the deformed central and outside wires. The initial core-wire clearance h_{i1} can be expressed in a form of a quadratic curve as follow

$$h_{i1}\left(y_{c1},z_{c1}\right)=\left(\frac{1}{\bar{R}_{1y_{c1}}}+\frac{1}{\bar{R}_{2y_{c1}}}\right)\frac{y_{c1}^2}{2} \tag{27}$$

where $\bar{R}_{1y_{c1}}$ and $\bar{R}_{2y_{c1}}$ are the y_{c1} directional radii of surface curvature of the central and outside wires at point o_{c1}. And the radius values are obtained with the relations $\bar{R}_{1y_{c1}}=\bar{R}_1/\cos^2\bar{\gamma}$ and $\bar{R}_{2y_{c1}}=\bar{R}_2/\cos^2\bar{\beta}$. Here, the angle variables $\bar{\gamma}$ and $\bar{\beta}$ are defined as $\bar{\gamma}=\pi/2-\arctan\left(\bar{p}_2/2\pi\bar{r}_{c1}\right)$ and $\bar{\beta}=\arctan\left(\bar{p}_2/2\pi\bar{r}_{c1}\right)-\bar{\alpha}_2$, respectively.

With respect to the contact between adjacent outside wires, the normal, binomial and tangential directions of the wire-wire contact line at an arbitrary point o_{c2} are denoted with lines $o_{c2}x_{c2}$, $o_{c2}y_{c2}$ and $o_{c2}z_{c2}$ in Fig. 4, respectively. Thus the wire-wire contact clearance h_{c2} at a point (y_{c2}, z_{c2}) on the y_{c2} axis is expressed as

$$h_{c2}\left(y_{c2},z_{c2}\right)=h_{i2}\left(y_{c2},z_{c2}\right)+u_2\left(y_{c2},z_{c2}\right)-u_2\left(0,z_{c2}\right) \tag{28}$$

where h_{i2} is the initial clearance between the adjacent outside wires. The symbol u_2 denotes the total elastic deformation of the wire-wire contact. The initial clearance h_{i2} can be expressed as

$$h_{i2}\left(y_{c2},z_{c2}\right)=\frac{y_{c2}^2}{\bar{R}_{2y_{c2}}} \tag{29}$$

where $\bar{R}_{2y_{c2}}$ is the radius of surface curvature of the outside wires at point o_{c2} along the y_{c2} direction, and $\bar{R}_{2y_c}=\bar{R}_2/\cos^2\bar{\theta}$.

Since the value of d_{s0} is taken to be small enough previously, the contact zone A_c between the chosen wire

sections can be treated as a rectangular one. Let $p(y_c, z_c)$ be the contact pressure at point (y_c, z_c), the load equilibrium yields

$$X_c d_{s0} = \int_{-\frac{d_{s0}}{2}}^{\frac{d_{s0}}{2}} \int_{-b}^{b} p(y_c, z_c) \mathrm{d}y_c \mathrm{d}z_c \tag{30}$$

Based on the minimum complementary energy principle, the interwire contact problem are reduced as the following extremum problem of a quadratic function (Hu et al., 1999):

$$\text{Minimize} \quad \mathbf{W}(\mathbf{p}) = \mathbf{h}_c^{\mathrm{T}} \cdot \mathbf{p} + \frac{1}{2} \mathbf{p}^{\mathrm{T}} \cdot \mathbf{I}_c \cdot \mathbf{p} \tag{31}$$

$$\text{subject to} \quad h_c(y_c, z_c) \geq 0, \ p(y_c, z_c) \geq 0, \ h_c(y_c, z_c) \cdot p(y_c, z_c) = 0 \tag{32}$$

where $\mathbf{W}$ is the objective function. The symbol $\mathbf{h}_c$ is the clearance matrix, $\mathbf{p}$ is the pressure matrix, and $\mathbf{I}_c$ is the influence coefficient matrix. The contact pressure and contact deformation can be obtained with the conjugate gradient method (CGM) and fast Fourier transform (FFT) adopted by the present authors (Meng et al., 2016). Eq. (32) shows that the contact pressure p is larger than zero when the clearance h_c=0. Inversely, if h_c>0, then p is equal to zero, implying the interwire separation.

In view of the non-conformal contact property of the strand (i.e., the dimension of the contact region is much smaller than those of the wires), the deformation u due to the contact pressure p can be calculated with Boussinesq theory (Johnson, 1985):

$$u(y_c, z_c) = \int_{-\frac{d_{s0}}{2}}^{\frac{d_{s0}}{2}} \int_{-\infty}^{\infty} G_u^p(y_c - y_c', z_c - z_c') p(y_c', z_c') \mathrm{d}y_c' \mathrm{d}z_c' \tag{33}$$

where the Green's function of the contact pressure for the deformation is G_u^p, and $G_u^p(y_c, z_c) = 1 \Big/ \left(\pi E^* \sqrt{y_c^2 + z_c^2} \right)$. The symbol E^* denotes the reduced Young's modulus. For the core-wire contact, $1/E^* = \left(1 - \nu_1^2\right)/E_1 + \left(1 - \nu_2^2\right)/E_2$. And for the wire-wire contact, $1/E^* = 2\left(1 - \nu_2^2\right)/E_2$. The deformations of the central and outside wires satisfy

$$\frac{\delta_1}{\delta_2} = \frac{\left(1 - \nu_1^2\right) E_2}{\left(1 - \nu_2^2\right) E_1} \tag{34}$$

In the present study, all wires are assumed to be made of the same material, i.e., E_1=E_2=E and ν_1=ν_2=ν for simplifying the calculation.

3. Numerical solution

3.1. Solution process

The key of solving the full contact model of the wire rope strand established in section 2 is the determination of the interwire contact status in the deformed state, due to the fact that the distribution of the load between the wires depends on the interwire contact status. A solution process based on a semi-analytical method (SAM) for the wire rope strand is proposed in the present study to realize the evaluation of the interwire contact behavior of the strand at varying loads. The overall solution process is shown in Fig. 5a, and the detailed numerical procedure is as follows:

Step 1. Assume that the core-wire contact status happens to the wire rope strand under a specific axial load (i.e., set the wire-wire contact deformation as zero), and solve the performance of the strand with the iterative solution process given in Fig. 5b, where the convergence precision ε_δ is set as 1.0×10^{-4}.

Step 2. Calculate the helix radius of the deformed outside wire centerline according to Eqs. (15a) and (15b), and judge whether the geometrical parameters after deformation satisfy the condition that the adjacent outside wires are not in contact (i.e., $\bar{r}_{\text{c-w}} > \bar{r}_{\text{w-w}}$). If the said condition is satisfied, then the interwire contact status at current load step is the core-wire contact status, and go to Step 6. Otherwise, go to Step 3.

Step 3. Assume that the wire-wire contact status happens (i.e., set the core-wire contact deformation as zero), and solve the strand performance with the iterative solution process given in Fig. 5b, where the convergence precision ε_δ is 1.0×10^{-4}.

Step 4. Calculate the helix radius of the deformed outside wire centerline according to Eqs. (15a) and (15b), and judge whether the parameters of the deformed strand satisfy the condition that the central and outside wires are not in contact (i.e., $\bar{r}_{\text{c-w}} < \bar{r}_{\text{w-w}}$). If the said condition is satisfied, then the interwire contact status at current load step is wire-wire contact, and go to Step 6. Otherwise, it indicates that the coupled-contact occurs.

Step 5. Solve the strand performance at the coupled-contact status with the solution process given in Fig.

5c, where the convergence precision ε_δ is 1.0×10^{-4}. Then terminate the solution at current load step.

Step 6. Increase the load if the maximum axial load on the strand is not reached and go to Step 1, otherwise terminate the total solution.

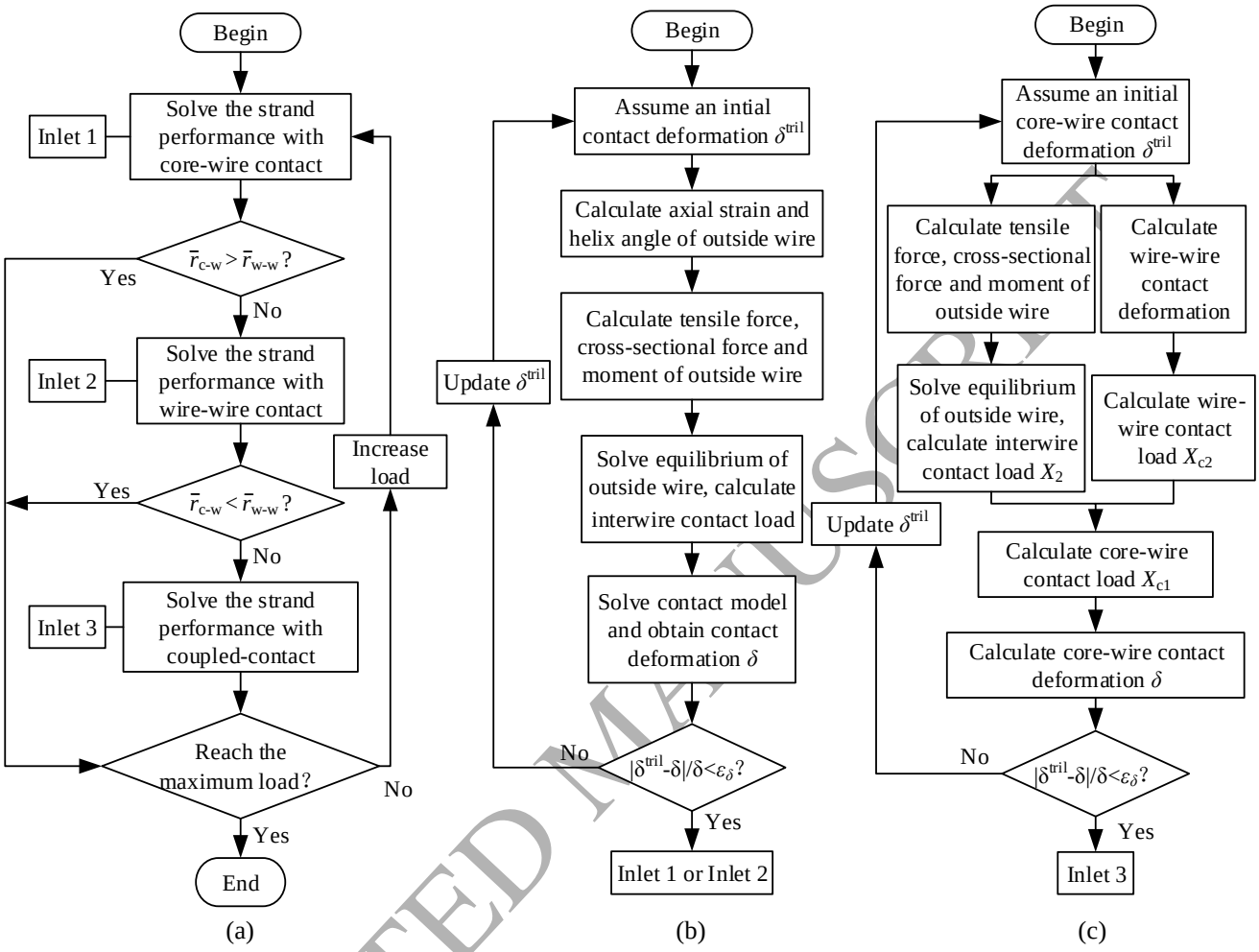

Fig. 5. Solution process for full contact model of wire rope strand. (a) Overall process. (b) Solution process in core-wire contact status or wire-wire contact status. (c) Solution process in coupled contact status.

3.2. Interwire contact solution

To realize the above-mentioned full contact solution process of the strand under varying loads, the interwire contact behavior should be computed. Considering the coupling relation between the contact pressure and contact deformation, an iterative procedure based on the conjugate gradient method (CGM) (Polonsky and Keer, 1999) is adopted. The computation domain is $\{(y_c, z_c)|-4b\le y_c\le 4b, -3b\le z_c\le 3b\}$, and discretized into the j_{max}(y_c direction)×k_{max}(z_c direction) elements, each of which the y_c- and z_c- directional dimensions are $\Delta y_c=8b/j_{max}$ and $\Delta z_c=6b/k_{max}$, respectively. Besides, the half-width of contact b is determined according to the location where interwire happens:

$$b = b_1 = \sqrt{\frac{4X_{c1}}{\pi E^* \left(\frac{\sin^2 \bar{\alpha}_2}{\bar{R}_1} + \frac{1}{\bar{R}_2} \right)}}, \text{ for core-wire contact} \tag{35a}$$

$$b = b_2 = \sqrt{\frac{2X_{c2}\bar{R}_2}{\pi E^*}}, \text{ for wire-wire contact} \tag{35b}$$

Similar to the dealing in early work of the present authors (Meng et al., 2016), the fast Fourier transform (FFT) (Liu et al., 2000) is adopted to calculate the contact deformation. This method can realize the quick and precise evaluation of the contact deformation due to its capacity of shorten the computation time. The contact deformation u is obtained with

$$u = \mathrm{IDFT}\left(\hat{\hat{I}}_c \cdot \hat{\hat{p}} \right) \tag{36}$$

where the symbol " $\hat{}$ " denotes a two-dimensional discrete Fourier transform (DFT), whose inverse operation is represented with "IDFT". The symbol I_c is the influence coefficient of the contact deformation due to the contact pressure p. Before the iteration for the interwire contact solution, the influence coefficient I_c is computed with the relation

$$I_c(j,k) = \int_{-\frac{\Delta z_c}{2}}^{\frac{\Delta z_c}{2}} \int_{-\frac{\Delta y_c}{2}}^{\frac{\Delta y_c}{2}} G_u^p(j\Delta y_c - y_c, k\Delta z_c - z_c)\,\mathrm{d}y_c\,\mathrm{d}z_c \tag{37}$$

where the integral of the Green's function G_u^p can be analytically derived (Love, 1929).

4. Model verification

Before the full contact analysis, the comparison between the maximum contact pressures and changes in helix radius of the outside wire by the present full contact model and the FEM result by Jiang et al. (Jiang et al., 2008) is given in Fig. 6, where the maximum core-wire contact pressure and the maximum wire-wire contact pressure are denoted with σ_{cw} and σ_{ww}, respectively. It should also be mentioned that a negative value of the change in helix radius in Fig. 6b indicates that the helix radius decreases. Meanwhile, the result only considering the contact between the central and outside wires (the core-wire contact model in Fig. 6), along with that obtained with the Costello's theory (Costello, 1997), is also presented. The results show that both the contact pressure in Fig. 6a and the change in helix radius (absolute value) in Fig. 6b, obtained with

the core-wire contact model, are larger than the corresponding values with the full contact model. The discrepancy can be explained with the fact the contact between adjacent outside wires ignored in the core-wire contact model weakens the core-wire contact load, thus making the distribution of interwire contact load more uniform. Neglecting the interwire contact deformation, as shown in Fig. 6b, the Costello's theory results in a much smaller change in helix radius than other methods. Moreover, it can be seen from Fig. 6a and b that the maximum contact pressure, and the change in helix radius by the present full contact model are in good accordance with the corresponding values by the FEM, which proves that the present model gives a precise solution of the interwire contact behavior of the wire rope strand.

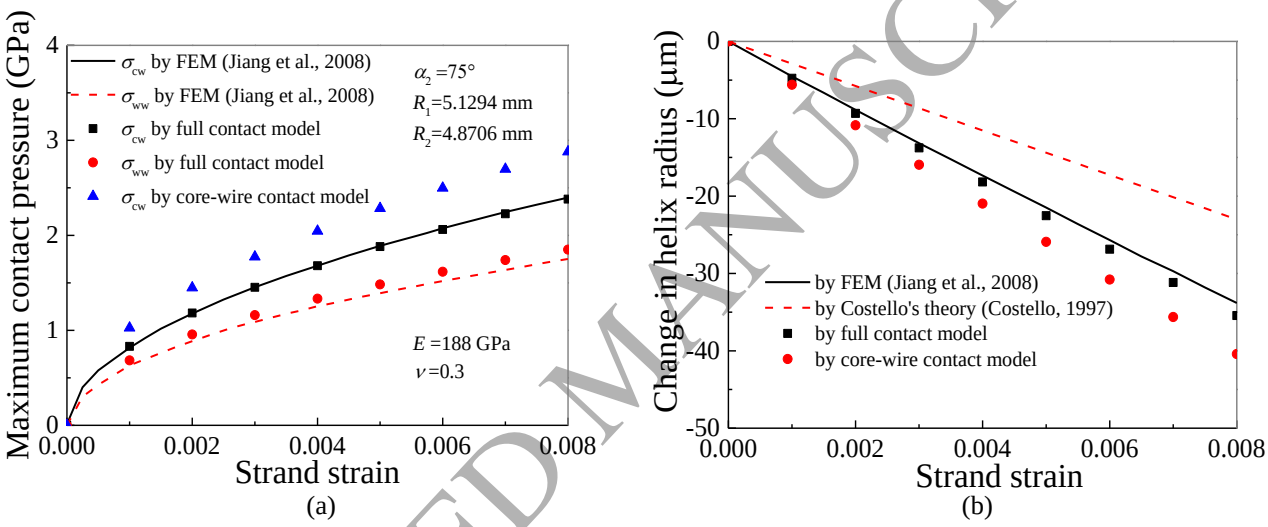

Fig. 6. Results comparison of strand in coupled contact. (a) Maximum contact pressure. (b) Change in helix radius of outside wire centerline.

Utting and Jones (1987) conducted axial tensile tests on simple straight strands with different end constraints (i.e., the nominal fixed-end, free-end and partial restraint). Torsional moment M in the nominal fixed-end condition, torsional strain τ_t in the free-end condition, along with the slopes of the torsional moment against the tensile and torsional strains in the partial constraint condition were obtained by them. In the present study, the axial tensile performance calculation of the strand with lay angles β of 17°, 12.2° and 9.2° (specimen I, IV and VI in the test by Utting and Jones) are made with the full contact model, and the comparison results are given in Tables 1 and 2. The parameters adopted for the comparison are as follows: R_1=1.97 mm, R_2=1.865 mm, E_1=E_2=197.9 GPa, ν_1=ν_2=0.3, and the axial tension F is 40 kN. Meanwhile, the torsional moment M and the torsional strain τ_t in the free-end condition by the present model in Table 1 are

respectively calculated according to the following relations:

$$M = \frac{k_{\theta\varepsilon}}{k_{\varepsilon\varepsilon}}\left(F - k_{\varepsilon\theta}\tau_{\mathrm{t}}\right) + k_{\theta\theta}\tau_{\mathrm{t}}, \text{ for fixed-end condition} \tag{38a}$$

$$\tau_{\mathrm{t}} = \frac{F}{k_{\varepsilon\theta} - \left(k_{\varepsilon\varepsilon}k_{\theta\theta}/k_{\theta\varepsilon}\right)}, \text{ for free-end condition} \tag{38b}$$

In Table 2, the slopes of the torsional moment against the tensile and torsional strains in the partial constraint condition are calculated with the following formulas:

$$\frac{\Delta M}{\Delta \varepsilon_{\mathrm{t}}} = k_{\theta\varepsilon} - \frac{k_{\varepsilon\varepsilon}k_{\theta\theta}}{k_{\varepsilon\theta}} \tag{39a}$$

$$\frac{\Delta M}{\Delta \tau_{\mathrm{t}}} = k_{\theta\theta} - \frac{k_{\theta\varepsilon}k_{\varepsilon\theta}}{k_{\varepsilon\varepsilon}} \tag{39b}$$

Meanwhile, the FEM result by Ghoreishi et al. (2007), the result obtained with an asymptotic method (AM) by Argatov (2011) as well as the present error relative to the AM result, are also given in Tables 1 and 2. The data in the tables shows that the present result matches well with the test data, FEM result and the AM result. The discrepancy between the present model, FEM and AM results from the different dealings of the interwire contact and friction. The FEM simulation by Ghoreishi et al. (2007) only considered the contact between the central and outside wires, and adopted a bonded contact model with an infinite friction assumption. Both the core-wire contact and the wire-wire contact are considered in the AM and the present model, and the interwire friction is also neglected in both models. Different from the AM, however, the present model fully considers the effect of the external load on the wire radius in the calculation of the bending and twist moments (expressed in Eq. (19)), which is thought to be more reasonable according to the real situation.

Table 1
Comparison of present model with experimental data (Utting and Jones, 1987), FEM result (Ghoreishi et al., 2007) and AM results (Argatov, 2011), for nominally fixed and completely free end conditions.

Specimen	M (N·m) (fixed-end)					τ_t (rad/m) (free-end)				
	Test	FEM	AM	Present	Error (%)	Test	FEM	AM	Present	Error (%)
I (β=17°)	34.4	36.7	38.8	37.9	-2.32	2.4929	2.50889	2.62040	2.57321	-1.80
IV (β=12.2°)	26	27.2	27.0	27.4	1.48	2.2049	2.12266	2.19051	2.17879	-0.54
VI (β=9.2°)	18.8	19.9	21.4	20.7	-3.27	1.62025	1.73139	1.78152	1.77556	-0.33

Table 2
Comparison of the present model with experimental data (Utting and Jones, 1987), FEM result (Ghoreishi et al., 2007) and AM results (Argatov, 2011), for partially strained ends.

Specimen	$\Delta M/\Delta\varepsilon_t$ (kN·m)					$\Delta M/\Delta\tau_t$ (N·m^2)				
	Test	FEM	AM	Present	Error (%)	Test	FEM	AM	Present	Error (%)
I (β=17°)	16.2	15.94	14.92	14.49	-2.88	13.7	15.03	14.46	14.71	1.73
IV (β=12.2°)	20.1	18.84	18.08	18.18	0.55	12.8	12.84	12.52	12.56	0.32
VI (β=9.2°)	22.9	23.1	22.34	22.34	0	11.6	11.92	11.64	11.65	0.09

For a further validation of the present model, the stiffness matrix of a wire rope strand obtained with the present model is compared with the experiment data by Kumar and Botsis (2001) and the AM results by Argatov (2011). The geometrical and material parameters for the comparison are as follows: R_1=1.5 mm, R_2=1.5 mm, E_1=E_2=E=157.0 GPa, ν_1=ν_2=0.3 and β=9.6°. The dimensionless stiffness values are given in Table 3, where the stiffnesses are defined as $\bar{k}_{\varepsilon\varepsilon}=k_{\varepsilon\varepsilon}/\left(EA_{\mathrm{n}}\right)$, $\bar{k}_{\varepsilon\theta}=k_{\varepsilon\theta}/\left(EA_{\mathrm{n}}R_{\mathrm{n}}\right)$, $\bar{k}_{\theta\varepsilon}=k_{\theta\varepsilon}/\left(ER_{\mathrm{n}}^3\right)$ and $\bar{k}_{\theta\theta}=k_{\theta\theta}/\left(ER_{\mathrm{n}}^4\right)$. The symbols A_{n} and R_{n} are the total cross-sectional area and the radius of the strand, and $A_n=\pi R_1^2+6\pi R_2^2$, R_n=R_1+2R_2. Table 3 shows that the present model gives results in better accordance with the experimental data, compared with the AM. Thus, with the consideration of the interaction between the interwire coupled contact behavior and the strand's axial mechanical performance, as well as the effect of the deformation on the wire's bending and twist moments, the established full contact model of wire rope strand is verified.

Table 3
Comparison of stiffness matrix by present model with reported results.

Relative stiffnesses	$\bar{k}_{\varepsilon\varepsilon}$	$\bar{k}_{\varepsilon\theta}$	$\bar{k}_{\theta\varepsilon}$	$\bar{k}_{\theta\theta}$
Experiment (Kumar and Botsis, 2001)	0.92	0.107	0.215	0.095
Asymptotic model (Argatov, 2011)	0.95	0.092	0.223	0.080
Present model	0.95	0.094	0.221	0.081

5. Results and discussion

5.1. Performance under varying axial tension

Based on the established full contact solution scheme, the interwire contact behavior and the axial mechanical performance of the strand under varying axial tensile load in fixed-end and free-end conditions are analyzed, which has not be realized with past models based on the assumption of constant interwire

contact status. The axial torsional strain of the strand τ_t is 0 rad/m in the axial tensile performance calculation under the fixed-end condition, while there is no axial torsion M acting on the strand under the free-end condition.

The maximum contact pressure σ and maximum contact deformation δ of the strands versus the strand tensile strain at different lay angles β are shown in Figs. 7-9, in which the subscripts "cw" and "ww" denote the core-wire contact and wire-wire contact, respectively. The results shows that the maximum values of the contact pressure and deformation under the free-end condition are smaller than the corresponding values under the fixed-end condition, which is due to that the strand rotates about its axis during the axial tension process under the free-end condition.

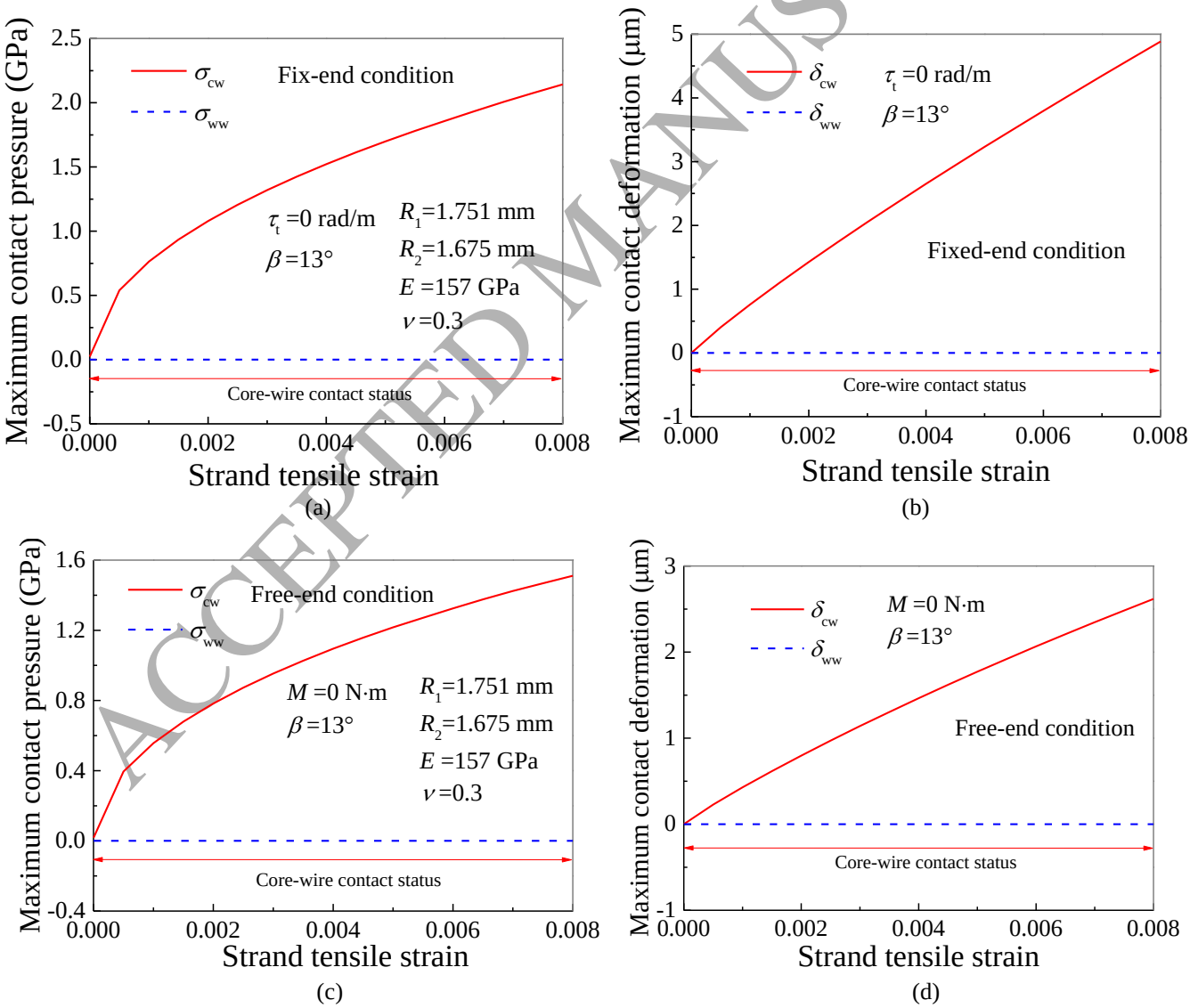

Fig. 7. Contact behavior evolution of strand subjected to varying axial tension (β=13°).
(a) Maximum contact pressure at fixed-end condition. (b) Maximum contact deformation at fixed-end condition.
(c) Maximum contact pressure at free-end condition. (d) Maximum contact deformation at free-end condition.

Figs. 7-9 show that the change rules of the contact behavior of the axially stretched strands with different lay angles are different. Under the fixed-end and free-end conditions, the strand with lay angle of 13° lies in the core-wire contact status throughout the tension process (see Fig. 7), and the strand with β=15° is in the wire-wire contact status (Fig. 8). Different from the behavior of the above two strands, the contact status of the strand with β=14° depends on the end condition. Under the fixed-end condition, the strand becomes a wire-wire contact status at the beginning of the axial tension, and changes to the coupled contact status at a certain axial strain (see Fig. 9a and b). As shown in Fig 9c and d, however, the change rule of the interwire contact status of the strand under free-end condition is complex. Only wire-wire contact happens first and then the coupled contact status occurs when the strain reaches about 0.0005, which is smaller than the strain for the contact status transformation under the fixed-end condition. As the axial tension goes on, the outside wires are apart from each other, and the strand turns into the core-wire contact status.

The above different evolutions result from the combined effect of the lay angle, the interwire contact deformation and the effect of the Poisson's ratio. Before the tensile loading, the interwire contact status depends only on the initial lay angle due to the fact that no interwire contact deformation happens and the axial strains of the wires are zero. The calculation from Eq. (14c) shows that the value of the critical lay angle for the strand is 13.893°, which means that the initial contact status of the strands with lay angles smaller or greater than the above critical angle is core-wire contact or wire-wire contact, respectively. Moreover, the initial coupled contact happens when the strand's lay angle equals the said critical lay angle. Once the axial tension is loaded, the interwire contact deformation and the radius shrinkage due to the effect of Poisson's ratio of the wires lead to the change in the strand's geometrical parameters including the lay angle and interwire clearance.

For the strand with initial core-wire contact, the radius shrinkage of the central wire and the contact deformation make the outside wire approaching the central wire and its adjacent outside wires. The effect of the radius shrinkage of the outside wire is complex. In view of that the central and outside wires are in

contact with each other, on the one hand, the radius shrinkage makes the central and outside wires approaching to each other, which makes the adjacent outside wires closer. On the other hand, however, the radius shrinkage increases the clearance between outside wires, which results in the separation tendency of the said wires. The above influencing factors codetermine the interwire contact status of the strand, which is judged with Eq. (14). The interwire contact status keeps the core-wire contact when the separation tendency of the outside wires is more obvious than the approaching tendency, as shown in Fig. 7. Thus the contact fatigue may happen at the contact interface between the central and outside wires of the strand under prolonged service. This is not noticed in the past strand researches due to their common assumption of the constant tension (Argatov, 2011; Ghoreishi et al., 2007).

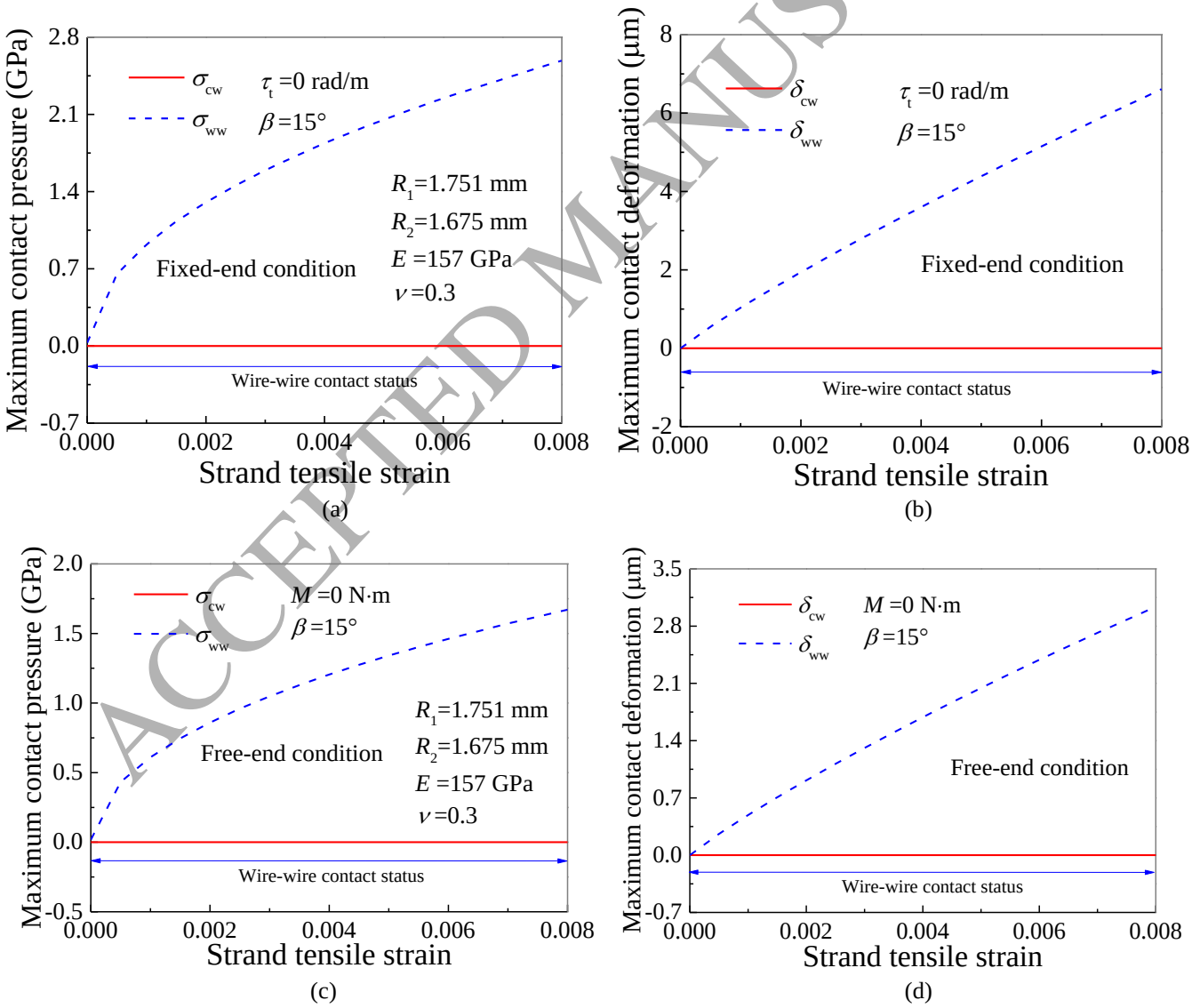

Fig. 8. Contact behavior evolution of strand subjected to varying axial tension (β=15°).
(a) Maximum contact pressure at fixed-end condition. (b) Maximum contact deformation at fixed-end condition.
(c) Maximum contact pressure at free-end condition. (d) Maximum contact deformation at free-end condition.

For the strand with initial wire-wire contact, the contact deformation and the radius shrinkage of the outside wire due to the Poisson's ratio make the adjacent outside wires closer, which results in the approaching tendency between the central and outside wires. However, the decrements in the radii of the central and outside wires lead to the separation between them. The core-wire contact status is kept if the separation tendency is dominant, as shown in Fig. 8. Therefore, the contact between adjacent outside wires results more easily in the interwire contact fatigue compared with the core-wire contact.

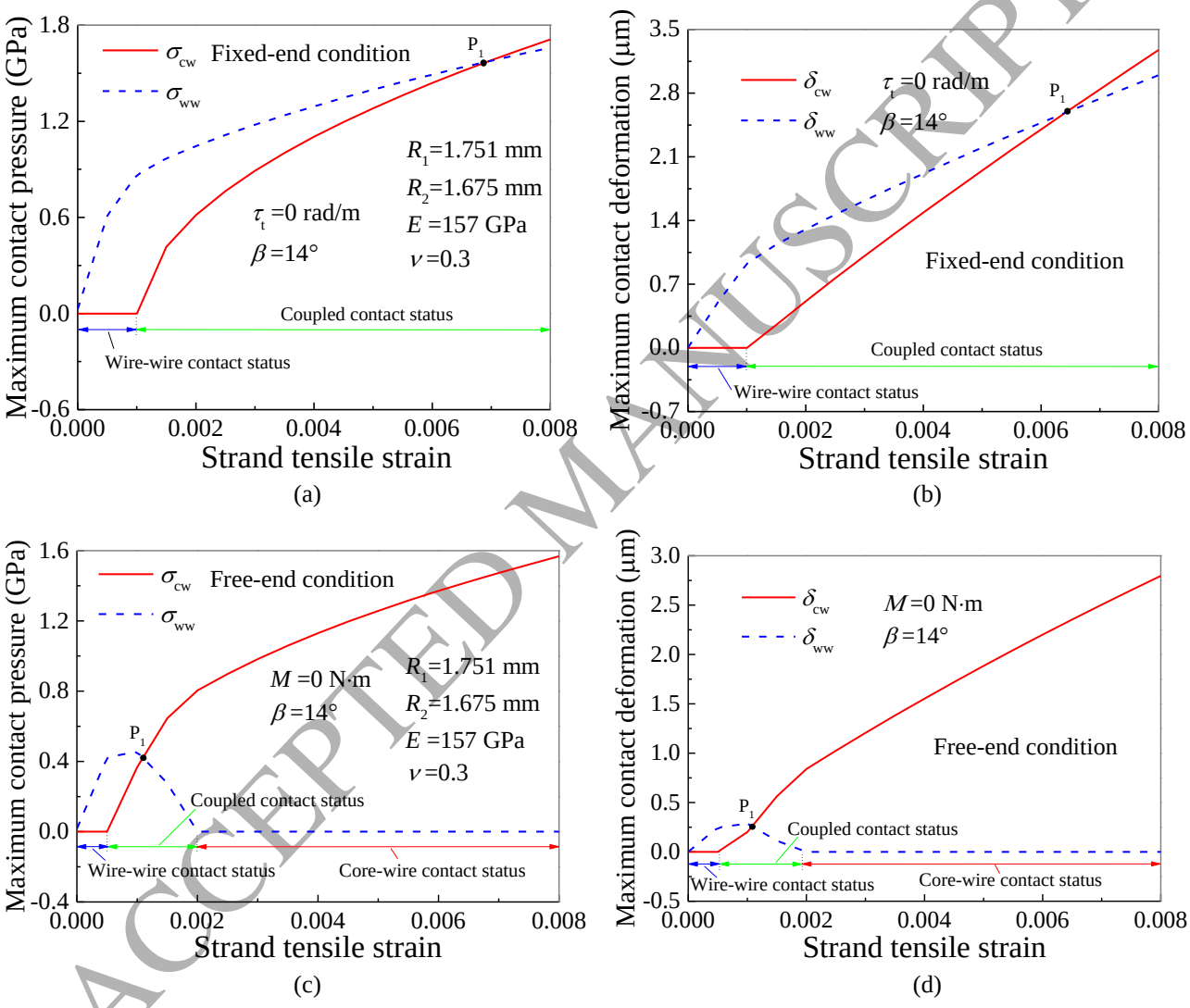

Fig. 9. Contact behavior evolution of strand subjected to varying axial tension (β=14°).
(a) Maximum contact pressure at fixed-end condition. (b) Maximum contact deformation at fixed-end condition.
(c) Maximum contact pressure at free-end condition. (d) Maximum contact deformation at free-end condition.

Fig. 9 shows that the contact between the central and outside wires happens at a certain axial strain, which means that the approaching tendency between the said wires is more obvious than the separation one. This phenomenon is not reported in the past researches (Argatov, 2011; Ghoreishi et al., 2007; Jiang et al., 2008; Stanova et al., 2015) with the assumption of constant interwire contact status. Meanwhile, it can also be seen

from this figure that the contact between the adjacent outside wires is dominant at the early stage of the coupled contact of the strand. As the axial tension continues, increasing rates of the contact pressure and deformation of the core-wire contact are larger than the corresponding values of the wire-wire contact, resulting in the phenomenon that the core-wire contact is dominant after the tensile strain reaches about 0.0069 and 0.001 (see the point P_1 in Fig. 9) under the fixed-end and free-end condition, respectively. Consequently, the region where the contact fatigue may happen depends on the end condition and the value of the axial strain. The contact fatigue may happen at both the interfaces of core-wire contact and wire-wire contact of the strand in a coupled contact status, and the most dangerous region transfers from the wire-wire contact interface to the core-wire contact interface as the tensile strain increases.

To study the axial mechanical performance of the wire rope strand under varying axial tension, the evolutions of the dimensionless tensile stiffness $\bar{k}_{\varepsilon\varepsilon}$ and coupling stiffness $\bar{k}_{\theta\varepsilon}$ of the strands with different lay angles are analyzed, which has not been realized in the past researches. As shown in Fig. 10, the dimensionless stiffnesses are respectively calculated with $\bar{k}_{\varepsilon\varepsilon} = k_{\varepsilon\varepsilon} \big/ \left(E\pi r_{\mathrm{h}2}^2 \right)$ and $\bar{k}_{\theta\varepsilon} = k_{\theta\varepsilon} \big/ \left(E\pi r_{\mathrm{h}2}^3 \right)$ (Ghoreishi et al., 2007). The results in this figure show that as the lay angle increases, the $\bar{k}_{\varepsilon\varepsilon}$ keeps decreasing but the $\bar{k}_{\theta\varepsilon}$ increases first and then decreases, indicating that there exists a critical angle that leads to a maximum value of $\bar{k}_{\theta\varepsilon}$. The obtained conclusion is in accordance with those in the past researches (Argatov, 2011; Ghoreishi et al., 2007) based on the assumption of constant interwire contact status. Besides this, the present results show that the axial tension also affects the strand stiffness, and the effect of the axial tension on the stiffnesses $\bar{k}_{\varepsilon\varepsilon}$ and $\bar{k}_{\theta\varepsilon}$ depends on the lay angle of the strand, which is not be calculated with the past researches (Argatov, 2011; Ghoreishi et al., 2007; Usabiaga and Pagalday, 2008) based on the constant interwire contact status. As the tensile strain increases, both $\bar{k}_{\varepsilon\varepsilon}$ and $\bar{k}_{\theta\varepsilon}$ at small lay angles keep stable values, while their values increase at large lay angles. With regard to the wire rope strands under varying axial tension, the increment of the load may cause changes in the strand stiffness, which should be considered in the design and analysis of the wire rope.

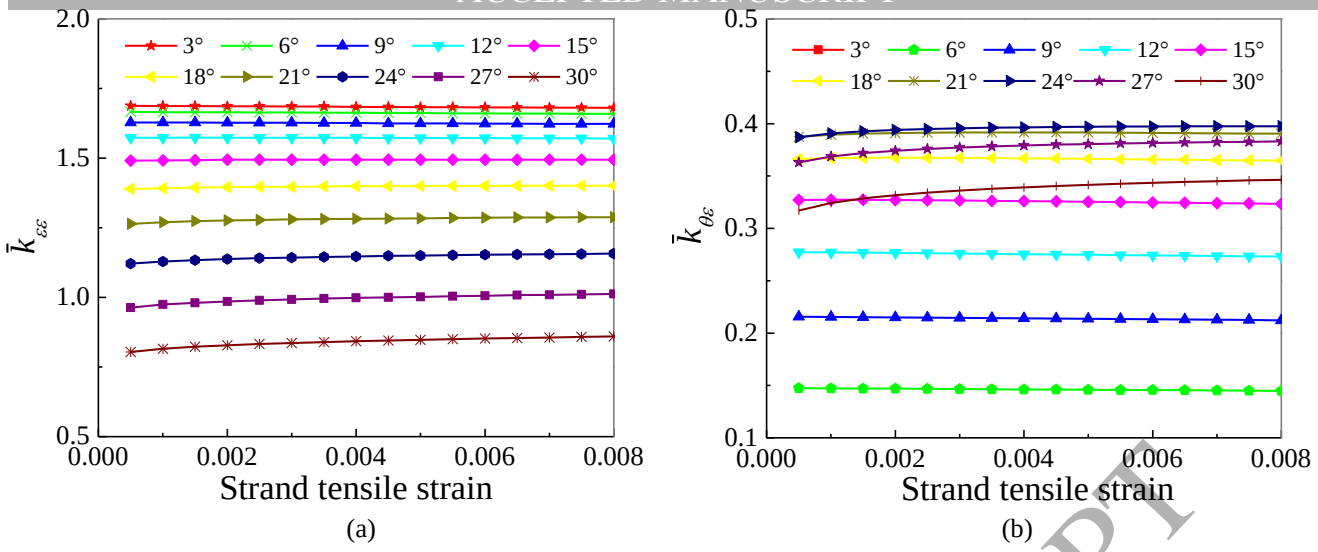

Fig. 10. Dimensionless stiffness evolution of strand subjected to varying axial tension. (a) Tensile stiffness $\bar{k}_{\varepsilon\varepsilon}$. (b) Coupling stiffness $\bar{k}_{\theta\varepsilon}$.

5.2. Performance under varying axial torsion

Beside of the axial tension, the axial torsion is also the common external load for wire ropes. The performance of the wire rope strand under varying axial torsion is studied with the full contact model in this section, which has not been analyzed in the past researches (Argatov, 2011; Ghoreishi et al., 2007; Jiang et al., 2008; Stanova et al., 2015). It should be mentioned that the direction of the axial torsion applied on the strand is the same as the lay direction, and the axial tensile strain ε_t of the strand keeps zero.

As an example, the contact behavior evolution of the strand with the lay angle β of 14° is given in Fig. 11. As the torsional strain increases, both the contact pressure σ and deformation δ due to the wire-wire contact increase and their values are positive, while the results due to the core-wire contact keep zero. This phenomenon indicates that the strand remains at the wire-wire contact status, and it can be explained according to the change in the helix radius of the outside wire centerline of the strand in Fig. 12. The positive result here shows that the central and outside wires are separating from each other under the axial torsion. As mentioned in section 5.1, the critical lay angle of the strand is 13.893° and thus the initial interwire contact status is the wire-wire contact. Consequently, the core-wire contact will not occur as the torsion continues. Moreover, it can be concluded that under the axial torsion, a strand with a lay angle larger than the critical lay angle keeps at the wire-wire contact status, implying the contact interfaces between the

outside wires in danger of contact fatigue failure.

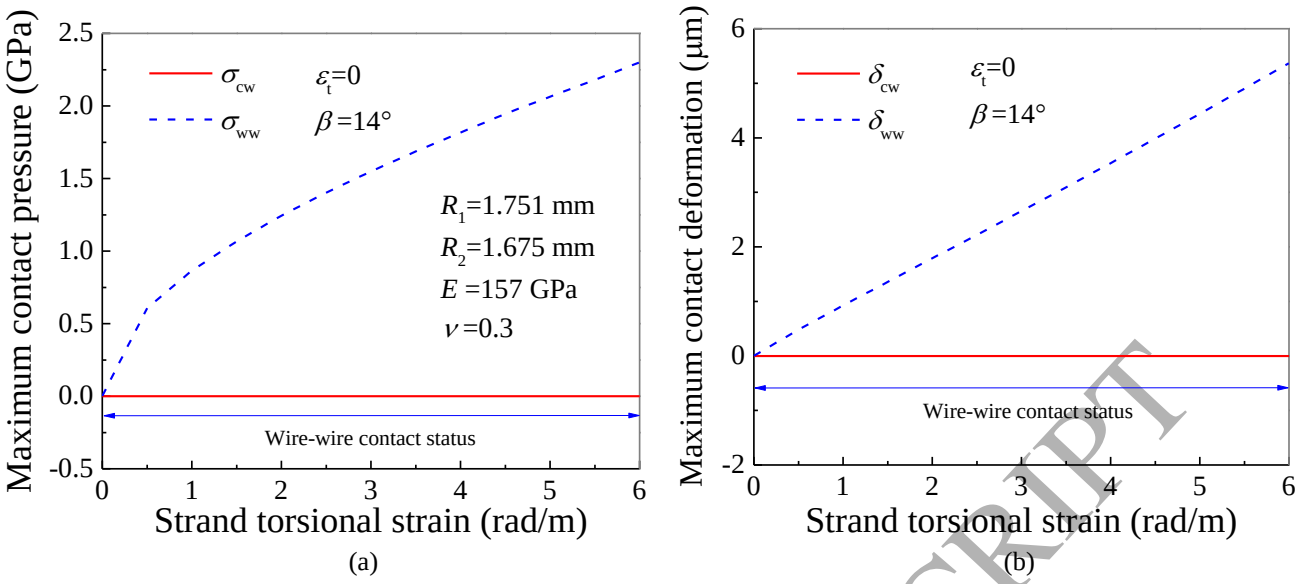

Fig. 11. Contact behavior evolution of strand subjected to varying axial torsion (β=14°).
(a) Maximum contact pressure. (b) Maximum contact deformation.

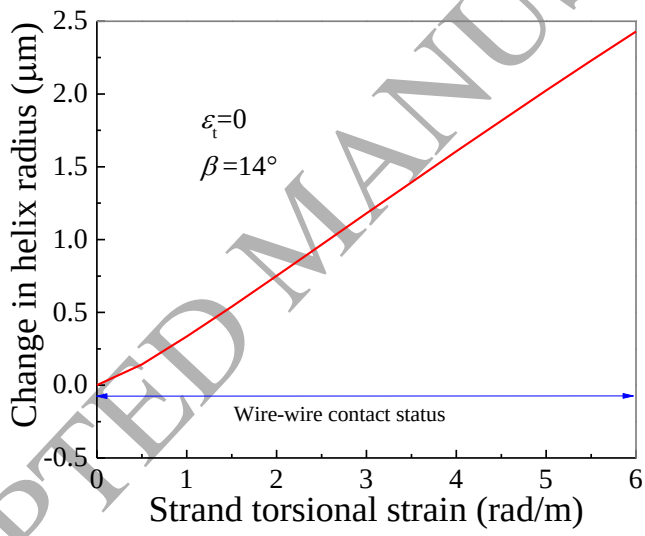

Fig. 12. Change in helix radius of outside wire centerline of strand subjected to varying axial torsion (β=14°).

Fig. 13 presents the contact behavior evolution of the strand with the lay angle of 13.5°. From the interwire contact pressure and contact deformation, it can be seen that the evolution of the interwire contact behavior of the strand is complex. This phenomenon has not been obtained in the past researches (Argatov, 2011; Ghoreishi et al., 2007; Jiang et al., 2008; Stanova et al., 2015) assuming constant interwire contact status. As stated previously, the strand is at initial core-wire contact status because its initial lay angle is smaller than the critical one. With the increment of the torsional strain, both the contact pressure and contact deformation due to the core-wire contact increase while those due to the wire-wire contact remain to be zero

in the beginning of the torsion process. The contact between adjacent outside wires happens when the torsion strain reaches about 1.5 rad/m, and the strand turns into the coupled contact status. As the axial torsion continues, the dominance of the core-wire contact is weakened, while the contact parameters due to the wire-wire contact increase. Then the core-wire contact and wire-wire contact are equal to each other at a center torsional strain (see point P_1 in Fig. 13), after which the wire-wire contact is dominant. At the stain of about 5.5 rad/m, the contact parameters due to the core-wire contact become zero, and the strand turns into the wire-wire contact status.

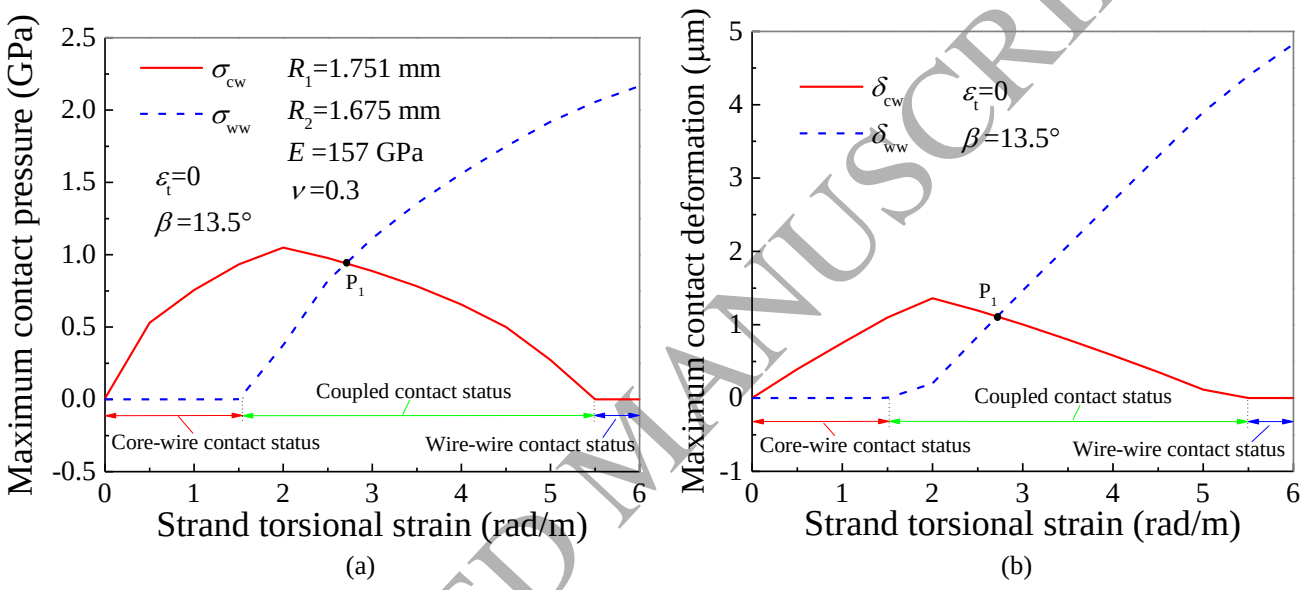

Fig. 13. Contact behavior evolution of strand subjected to varying axial torsion (β=13.5°).
(a) Maximum contact pressure. (b) Maximum contact deformation.

For purpose of further discussion, the change in the helix radius of outside wire of the strand is given in Fig. 14. It can be found from this figure that the curve for the change in the helix radius has two turning points (see points A and B in Fig. 14), which are caused by the change of the interwire contact status. At the stage of the core-wire contact status, the negative value of the change in the helix radius indicates that the central and outside wires are approaching to each other, which is due to increasing contact deformation and radius shrinkage. Meanwhile, the adjacent outside wires are getting closer due to decreasing helix radius and increasing lay angle caused by the torsion. After the strand turns into the coupled contact status, the core-wire contact effect is weakened along with the increasing wire-wire contact interaction caused by the torsion. Thus the core-wire contact deformation decreases and the central and outside wires are separating

(see the variation trend of values on line AB reflecting the coupled contact status in Fig. 14), which finally causes the second turning point B of the curve. From the results obtained with the full contact scheme, consequently, it can be concluded that the axial torsion can lead to an obvious change of the interwire contact behavior, which is not discovered with the past researches (Argatov, 2011; Ghoreishi et al., 2007; Jiang et al., 2008; Stanova et al., 2015). And the wire-wire contact is dominant for the strand under a large axial torsion.

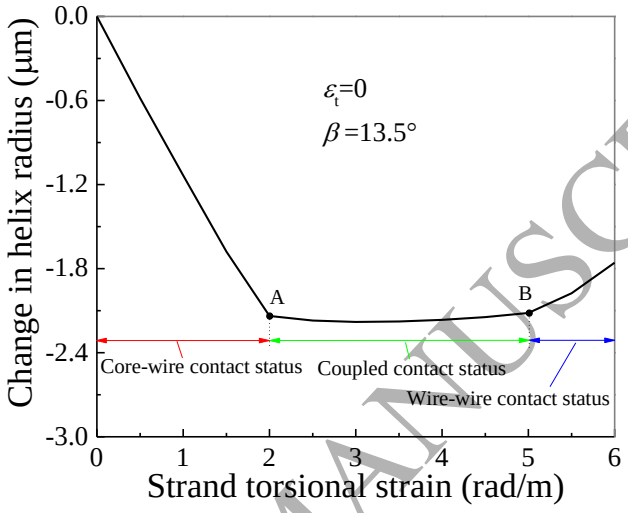

Fig. 14. Change in helix radius of outside wire centerline of strand subjected to varying axial torsion (β=13.5°).

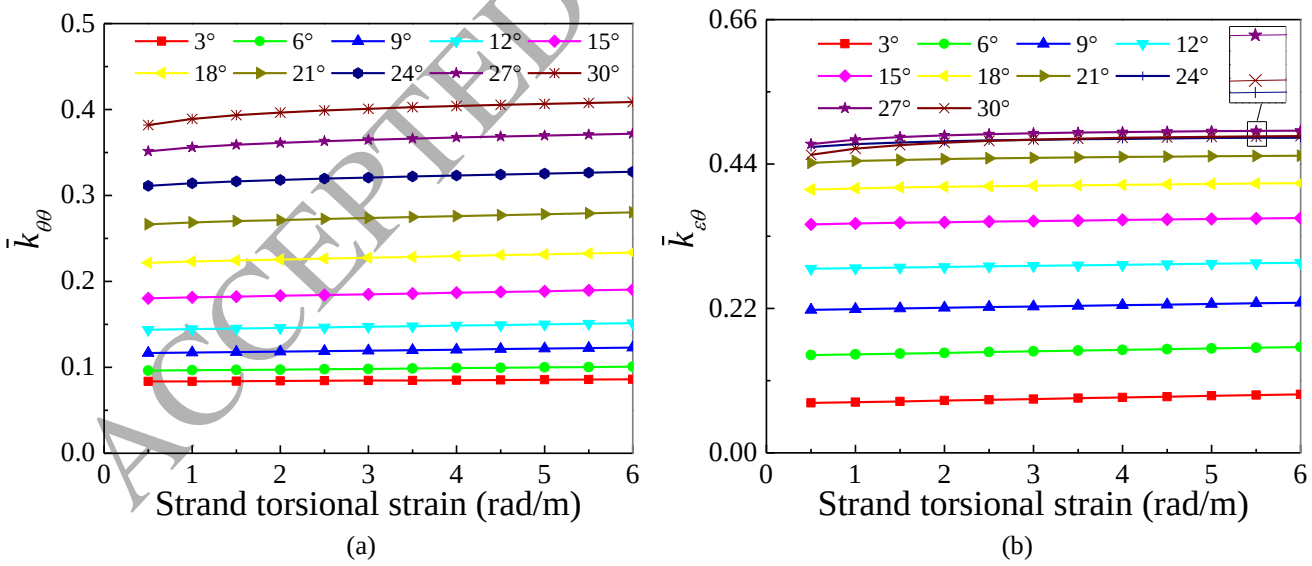

Fig. 15. Dimensionless stiffness evolution of strand subjected to axial torsion.
(a) Torsional stiffness $\bar{k}_{\theta\theta}$. (b) Coupling stiffness $\bar{k}_{\varepsilon\theta}$.

Under the condition of varying axial torsional moment, the dimensionless stiffness evolutions of the strands with different lay angles are illustrated in Fig. 15. The dimensionless torsional stiffness $\bar{k}_{\theta\theta}$ and the

coupling stiffness $\bar{k}_{\varepsilon\theta}$ are respectively defined as $\bar{k}_{\theta\theta} = k_{\theta\theta} / \left(E\pi r_{\mathrm{h}2}^4 \right)$ and $\bar{k}_{\varepsilon\theta} = k_{\varepsilon\theta} / \left(E\pi r_{\mathrm{h}2}^3 \right)$ (Ghoreishi et al., 2007). From the figure, it can be seen that an increment in the lay angle of the strand leads to a larger torsional stiffness. However, the coupling stiffness increases first and then decreases as the lay angle increases. These rules accord with the conclusions achieved in literatures (Argatov, 2011; Ghoreishi et al., 2007), in which the assumption of constant interwire contact status was adopted but the effect of the torsion on the strand stiffness was ignored. Obtained with the present full contact scheme, moreover, the evolutions of the stiffnesses at different lay angles are different. As the axial torsion goes on, the stiffnesses at small lay angles almost keep constant and the strands perform stable behavior, while obvious stiffness enhancements happen to the strands with large lay angles. From Figs. 10 and 15, it can be concluded that both the varying axial tension and torsion can lead to a change in the stiffness of the strand, and the effect of the axial loads on the strand performance should be taken into consideration, especially for the strand with a large lay angle.

6. Conclusions

In this paper, the full contact research of the wire rope strand under varying axial tension and torsion are made with the semi-analytical method (SAM). In doing so, an interwire full contact model considering different contact statuses is established based on contact mechanic and thin rods theories, and solved with the SAM in which the conjugate gradient method (CGM) and fast Fourier transform (FFT) are used for evaluating interwire contact performances. Then the evolutions of the interwire contact pressure, deformation and the stiffness of the strands with different lay angles are analyzed, and the associated conclusions are given below.

1) The proposed interwire contact scheme can effectively analyze contact performances at different contact statuses of the strand subjected to varying loads, which is not achieved with the contact methods in the past researches.
2) The full contact research shows that as the lay angle increases, the tensile stiffness decreases, torsional stiffness increases, while the coupling stiffnesses increase first and then decrease, which coincides with

the conclusions with past models. Moreover, it is discovered with the proposed model that as the axial loading process continues, the stiffness at a small lay angle keeps stable, while the stiffness at a large lay angle increases obviously.

3) The progressive loading solution based on the full contact scheme shows that the core-wire contact is dominant for the small lay angle strands under a large axial tension, while the wire-wire contact is dominant for the stretched strands with large lay angles. A large axial torsion is likely to cause the wire-wire contact status of the strand, and the coupled contact status happens to the strands under some certain axial loads.

4) The full contact research shows that the external axial tensile and torsional loads have different effects on the interwire contact behavior of the strand. The axial tension makes the central and outside wires closer, while the axial torsion leads to the approach between adjacent outside wires.

Acknowledgments

The authors sincerely express their gratitude to anonymous reviewers for their suggestions in improving the manuscript. The present study was supported by the National Key Basic Research Program of China (973) (2014CB049403).

Conflict of interest

None declared.

References

Argatov, I., 2011. Response of a wire rope strand to axial and torsional loads: Asymptotic modeling of the effect of interwire contact deformations. Int. J. Solids Struct. 48 (10), 1413-1423.

Chen, Y.P., Meng, F.M., Gong, X.S., 2015. Parametric modeling and comparative finite element analysis of spiral triangular strand and simple straight strand. Adv. Eng. Softw. 90, 63-75.

Costello, G.A., 1983. Stresses in multilayered cables. J. Energ. Resour.-T. ASME 105 (3), 337-340.

Costello, G.A., 1997. Theory of wire rope. Springer, New York.

Elata, D., Eshkenazy, R., Weiss, M.P., 2004. The mechanical behavior of a wire rope with an independent wire rope core. Int. J. Solids Struct. 41 (5-6), 1157-1172.

Erdonmez, C., Imrak, C.E., 2011. A finite element model for independent wire rope core with double helical geometry subjected to axial loads. Sadhana 36 (6), 995-1008.

Feyrer, K., 2007. Wire ropes: Tension, endurance, reliability. Springer, Berlin.

Fontanari, V., Benedetti, M., Monelli, B.D., 2015. Elasto-plastic behavior of a Warrington-Seale rope: Experimental analysis and finite element modeling. Eng. Struct. 82, 113-120.

Frikha, A., Cartraud, P., Treyssede, F., 2013. Mechanical modeling of helical structures accounting for translational invariance. Part 1: Static behavior. Int. J. Solids Struct. 50 (9), 1373-1382.

Ghoreishi, S.R., Messager, T., Cartraud, P., Davies, P., 2007. Validity and limitations of linear analytical models for steel wire strands under axial loading, using a 3D FE model. Int. J. Mech. Sci. 49 (11), 1251-1261.

Gnanavel, B.K., Gopinath, D., Parthasarathy, N.S., 2010. Effect of friction on coupled contact in a twisted wire cable. J. Appl. Mech.-T. ASME 77 (2), 293-298.

Hruska, F.H., 1952. Radial forces in wire ropes. Wire and Wire Products 27 (5), 459-463.

Hruska, F.H., 1953. Tangential forces in wire ropes. Wire and Wire Products 28 (5), 455-460.

Hu, Y.Z., Barber, G.C., Zhu, D., 1999. Numerical analysis for the elastic contact of real rough surfaces.

Tribol. T 42 (3), 443-452.

Inagaki, K., Ekh, J., Zahrai, S., 2007. Mechanical analysis of second order helical structure in electrical cable. Int. J. Solids Struct. 44 (5), 1657-1679.

Jiang, W.G., 2012. A concise finite element model for pure bending analysis of simple wire strand. Int. J. Mech. Sci. 54 (1), 69-73.

Jiang, W.G., Henshall, J.L., 1999. The analysis of termination effects in wire strand using the finite element method. J. Strain Anal. Eng. Des. 34 (1), 31-38.

Jiang, W.G., Warby, M.K., Henshall, J.L., 2008. Statically indeterminate contacts in axially loaded wire strand. Eur. J. Mech. A. Solids 27 (1), 69-78.

Jiang, W.G., Yao, M.S., Walton, J.M., 1999. A concise finite element model for simple straight wire rope strand. Int. J. Mech. Sci. 41 (2), 143-161.

Johnson, K.L., 1985. Contact mechanics. Cambridge University Press, Cambridge.

Jolicoeur, C., Cardou, A., 1991. A numerical comparison of current mathematical-models of twisted wire cables under axisymmetrical loads. J. Energ. Resour.-T. ASME 113 (4), 241-249.

Karathanasopoulos, N., 2015. Torsional stiffness bounds of helical structures under the influence of kinematic constraints. Structures 3, 244-249.

Karathanasopoulos, N., Angelikopoulos, P., 2016. Optimal structural arrangements of multilayer helical assemblies. Int. J. Solids Struct. 78-79, 1-8.

Kumar, K., Botsis, J., 2001. Contact stresses in multilayered strands under tension and torsion. J. Appl. Mech. 68 (3), 432-440.

Kumar, K., Cochran, J.E., 1987. Closed-form analysis for elastic deformations of multilayered strands. J. Appl. Mech.-T. ASME 54 (4), 898-903.

Liu, S.B., Wang, Q., Liu, G., 2000. A versatile method of discrete convolution and FFT (DC-FFT) for contact analyses. Wear 243 (1-2), 101-111.

Love, A.E., 1929. The stress produced in a semi-infinite solid by pressure on part of the boundary. Philosophical Transactions of the Royal Society A: Mathematical, Physical and Engineering Sciences 228, 377-420.

Love, A.E.H., 1944. A treatise on the mathematical theory of elasticity. Dover Publications, New York.

Machida, S., Durelli, A.J., 1973. Response of a strand to axial and torsional displacements. J. Mech. Eng. Sci. 15 (4), 241-251.

Mcconnell, K.G., Zemke, W.P., 1982. A model to predict the coupled axial torsion properties of ACSR electrical conductors. Exp. Mech. 22 (7), 237-244.

Meng, F.M., Chen, Y.P., Du, M.G., Gong, X.S., 2016. Study on effect of inter-wire contact on mechanical performance of wire rope strand based on semi-analytical method. Int. J. Mech. Sci. 115–116, 416-427.

Paczelt, I., Beleznai, R., 2011. Nonlinear contact-theory for analysis of wire rope strand using high-order approximation in the FEM. Comput. Struct. 89 (11-12), 1004-1025.

Polonsky, I.A., Keer, L.M., 1999. A numerical method for solving rough contact problems based on the multi-level multi-summation and conjugate gradient techniques. Wear 231 (2), 206-219.

Prakash, A., Conway, T.A., Costello, G.A., 1992. Compression of a cord. J. Appl. Mech.-T. ASME 59 (2S), S213-S216.

Ramsey, H., 1988. A theory of thin rods with application to helical constituent wires in cables. Int. J. Mech. Sci. 30 (8), 559-570.

Samras, R.K., Skop, R.A., Milburn, D.A., 1974. An analysis of coupled extensional-torsional oscillations in wire rope. J. Eng. Ind.-T. ASME 96 (4), 1130-1135.

Sathikh, S., Moorthy, M.B.K., Krishnan, M., 1996. A symmetric linear elastic model for helical wire strands under axisymmetric loads. J. Strain Anal. Eng. Des. 31 (5), 389-399.

Spak, K., Agnes, G., Inman, D., 2013. Cable modeling and internal damping developments. Appl. Mech. Rev. 65 (1), 69-126.

Stanova, E., Fedorko, G., Kmet, S., Molnar, V., Fabian, M., 2015. Finite element analysis of spiral strands with different shapes subjected to axial loads. Adv. Eng. Softw. 83, 45-58.

Usabiaga, H., Ezkurra, M., Madoz, M.A., Pagalday, J.M., 2008. Experimental test for measuring the normal and tangential line contact pressure between wire rope and sheaves. Exp. Techniques 32 (5), 34-43.

Usabiaga, H., Pagalday, J.M., 2008. Analytical procedure for modelling recursively and wire by wire stranded ropes subjected to traction and torsion loads. Int. J. Solids Struct. 45 (21), 5503-5520.

Utting, W.S., Jones, N., 1987. The response of wire rope strands to axial tensile loads-Part I. Experimental results and theoretical predictions. Int. J. Mech. Sci. 29 (9), 605-619.

Wang, X.Y., Meng, X.B., Wang, J.X., Sun, Y.H., Gao, K., 2015. Mathematical modeling and geometric analysis for wire rope strands. Appl. Math. Model. 39 (3-4), 1019-1032.

Xiang, L., Wang, H.Y., Chen, Y., Guan, Y.J., Wang, Y.L., Dai, L.H., 2015. Modeling of multi-strand wire ropes subjected to axial tension and torsion loads. Int. J. Solids Struct. 58 (3), 233-246.

Yu, Y.J., Chen, Z.H., Liu, H.B., Wang, X.D., 2014. Finite element study of behavior and interface force conditions of seven-wire strand under axial and lateral loading. Constr. Build. Mater. 66, 10-18.

List of Tables

Figure captions

Fig. 1. Geometrical features. (a) Wire rope strand. (b) Outside wire centerline.

Fig. 2. Interwire contact statuses of wire rope strand. (a) Core-wire contact status. (b) Wire-wire contact status. (c) Coupled contact status.

Fig. 3. Schematic of wire-wire contact. (a) Deformation relation. (b) Cross-section of strand.

Fig. 4. Schematic of outside wire centerline and interwire contact lines.

Fig. 5. Solution process for full contact model of wire rope strand. (a) Overall process. (b) Solution process in core-wire contact status or wire-wire contact status. (c) Solution process in coupled contact status.

Fig. 6. Results comparison of strand in coupled contact. (a) Maximum contact pressure. (b) Change in helix radius of outside wire centerline.

Fig. 7. Contact behavior evolution of strand subjected to varying axial tension (β=13°). (a) Maximum contact pressure at fixed-end condition. (b) Maximum contact deformation at fixed-end condition. (c) Maximum contact pressure at free-end condition. (d) Maximum contact deformation at free-end condition.

Fig. 8. Contact behavior evolution of strand subjected to varying axial tension (β=15°). (a) Maximum contact pressure at fixed-end condition. (b) Maximum contact deformation at fixed-end condition. (c) Maximum contact pressure at free-end condition. (d) Maximum contact deformation at free-end condition.

Fig. 9. Contact behavior evolution of strand subjected to varying axial tension (β=14°). (a) Maximum contact pressure at fixed-end condition. (b) Maximum contact deformation at fixed-end condition. (c) Maximum contact pressure at free-end condition. (d) Maximum contact deformation at free-end condition.

Fig. 10. Dimensionless stiffness evolution of strand subjected to varying axial tension. (a) Tensile stiffness $\bar{k}_{\varepsilon\varepsilon}$. (b) Coupling stiffness $\bar{k}_{\theta\varepsilon}$.

Fig. 11. Contact behavior evolution of strand subjected to varying axial torsion (β=14°). (a) Maximum contact pressure. (b) Maximum contact deformation.

Fig. 12. Change in helix radius of outside wire centerline of strand subjected to varying axial torsion (β=14°).

Fig. 13. Contact behavior evolution of strand subjected to varying axial torsion (β=13.5°). (a) Maximum contact pressure. (b) Maximum contact deformation.

Fig. 14. Change in helix radius of outside wire centerline of strand subjected to varying axial torsion

(β=13.5°).

Fig. 15. Dimensionless stiffness evolution of strand subjected to axial torsion. (a) Torsional stiffness $\bar{k}_{\theta\theta}$. (b) Coupling stiffness $\bar{k}_{\varepsilon\theta}$.